Neurobiology of Disease 177 (2023) 105981

Contents lists available at ScienceDirect

Neurobiology of Disease

journal homepage: www.elsevier.com/locate/ynbdi

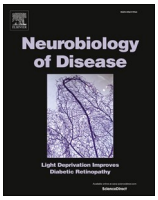

Local diffusion in the extracellular space of the brain

Jan Tønnesen [a,b,c], Sabina Hrabětová [d,e], Federico N. Soria [a,b,c,f,*]

[a] Achucarro Basque Center for Neuroscience, Leioa, Spain
[b] Department of Neuroscience, University of the Basque Country (UPV/EHU), Leioa, Spain
[c] Aligning Science Across Parkinson's (ASAP) Collaborative Research Network, Chevy Chase, MD 20815, USA
[d] Department of Cell Biology, State University of New York, Downstate Health Sciences University, Brooklyn, NY, USA
[e] The Robert F. Furchgott Center for Neural and Behavioral Science, State University of New York Downstate Health Sciences University, Brooklyn, NY, USA
[f] Centro de Investigación Biomédica en Red Enfermedades Neurodegenerativas (CIBERNED), Spain

ARTICLE INFO

Keywords:
Brain extracellular space
Interstitial fluid
Brain parenchyma
Extracellular matrix
Diffusion

ABSTRACT

The brain extracellular space (ECS) is a vast interstitial reticulum of extreme morphological complexity, composed of narrow gaps separated by local expansions, enabling interconnected highways between neural cells. Constituting on average 20% of brain volume, the ECS is key for intercellular communication, and understanding its diffusional properties is of paramount importance for understanding the brain. Within the ECS, neuroactive substances travel predominantly by diffusion, spreading through the interstitial fluid and the extracellular matrix scaffold after being focally released. The nanoscale dimensions of the ECS render it unresolvable by conventional live tissue compatible imaging methods, and historically diffusion of tracers has been used to indirectly infer its structure. Novel nanoscopic imaging techniques now show that the ECS is a highly dynamic compartment, and that diffusivity in the ECS is more heterogeneous than anticipated, with great variability across brain regions and physiological states. Diffusion is defined primarily by the local ECS geometry, and secondarily by the viscosity of the interstitial fluid, including the obstructive and binding properties of the extracellular matrix. ECS volume fraction and tortuosity both strongly determine diffusivity, and each can be independently regulated e.g. through alterations in glial morphology and the extracellular matrix composition. Here we aim to provide an overview of our current understanding of the ECS and its diffusional properties. We highlight emerging technological advances to respectively interrogate and model diffusion through the ECS, and point out how these may contribute in resolving the remaining enigmas of the ECS.

1. The brain extracellular space is a dynamic microenvironment

In aqueous medium, small particles move randomly by Brownian motion, as they collide with the water molecules surrounding them. This phenomenon is the basis of diffusion, which is the primary mechanism governing the movement of molecules over the short distances between cells. With the exception of ions or molecules moving through gap junctions, all intercellular signalling of the brain takes place through the narrow interconnected compartments that constitute the extracellular space (ECS). Diffusion within the ECS is therefore critical for neural function, and its study has captivated a niche of devoted researchers for >60 years. Along this journey, it has remained technically challenging to describe accurately the ECS structure. On one hand, the minute widths of the individual ECS channels –only a few tens of nanometres wide– defy the spatial resolution of conventional light microscopy, while on the other, standard sample preparation techniques for electron microscopy alter substantially ECS geometry and overall structure. Recent developments in light and electron microscopy provide nowadays a clearer picture of the ECS, enabling a more precise assessment of its topology and diffusive properties (Soria et al., 2020a).

As the ECS is confined by structurally dynamic cells, the ECS itself is an inherently dynamic compartment. ECS dynamics may result from the relatively fast protraction or retraction of microglial processes, structurally plastic myelin sheaths, or neuronal and astrocyte swelling, which are all commonly and constantly occurring phenomena. These structural dynamics span various timescales, ranging from hours, as in the case of sleep-wake cycle (Xie et al., 2013), to seconds in the case of epilepsy (Colbourn et al., 2021). The ECS channels, thus, increase and decrease in width, which conceivably toggle channels between open states and blind passages, so-called "dead-space microdomains". These local ECS

* Corresponding author at: Achucarro Basque Center for Neuroscience, Leioa, Spain.
E-mail address: federico.soria@achucarro.org (F.N. Soria).

https://doi.org/10.1016/j.nbd.2022.105981
Received 15 October 2022; Received in revised form 23 December 2022; Accepted 25 December 2022
Available online 26 December 2022
0969-9961/© 2022 The Authors. Published by Elsevier Inc. This is an open access article under the CC BY license (http://creativecommons.org/licenses/by/4.0/).

changes transiently alter the molecular diffusion paths, with consequences for neuronal activity and information processing.

The geometric structure of the ECS is not the only dynamic parameter that may influence diffusion. A major interstitial fluid (ISF) constituent, the extracellular matrix (ECM), undergoes continuous turnover and acts as a plastic diffusional barrier that changes qualitatively and quantitatively, including under pathological conditions (Krishnaswamy et al., 2019; Lau et al., 2013; Vargová and Syková, 2014). The ECM is anchored to cellular membranes by a hyaluronan backbone interlaced by proteoglycans and linker proteins. It forms a hygroscopic gel-like meshwork that serves both as ECS scaffold and as signalling hub (Dityatev et al., 2010b; Gaudet and Popovich, 2014). The ISF, which is in essence cerebrospinal fluid modified by the signalling and metabolic processes of the neuropil, fills the ECS and serves as the transport medium for the solutes and metabolites essential for collective cell function. These are transported within the narrow interstitial spaces, and through the larger perivascular space, which is basically an extension of the brain ECS. This *perivascular ECS* is associated with capillaries and other vessels, and is essential for diffusion between the brain interstitium and blood circulation (Pizzo and Thorne, 2017).

With its system of interconnected compartments, the ECS is thus a never-ending reservoir for diffusing ions and signalling molecules and a conduit for waste products that reflects the metabolic and communicational status of the surrounding cells. This *brain extracellular microenvironment* –i.e. the ECS and its constituent ISF and ECM– is, thus, a key component for brain function and its tight regulation. The ECS represents, on average, 20% of total brain volume in adult mammals and 40% in the neonatal brain (Syková and Nicholson, 2008). Understanding its dynamics, and especially how they affect the diffusion of molecules, is critical to understand how the brain works, and therefore how can we solve its problems when pathology ensues.

Here we aim to provide an overview of our current understanding of the ECS and its diffusional properties, highlighting recent advances in microscopy and mathematical diffusion models. We focus on local diffusion in interstitial spaces, across nano- to micrometers, as we consider it likely that these are the scales where the majority of signalling molecules exert their effect. We will not address the movement of fluid by convective *bulk flow*, as the importance of this is still being debated and because it expectedly becomes less important on smaller spatial scales compared to diffusion. There is experimental support for bulk flow in periarterial spaces, though it remains unclear whether it contributes to the transport of substances through interstitial spaces. There is an opportunity for a new avenue of research that would address this question experimentally. Readers interested in bulk flow and the controversy about the *glymphatic hypothesis* and related concepts are referred to recent literature (Abbott et al., 2018; Bohr et al., 2022; Hladky and Barrand, 2022; Rasmussen et al., 2018), including a review article in this issue of *Neurobiology of Disease*. We conclude the review by identifying unsolved questions in the field, and suggesting how future developments may be implemented to tackle them.

2. What does the brain ECS look like?

It is understandable that simultaneously (or even prior) to the study of how molecules move through the ECS, researchers have also tried to image it and visualize its structure. As we mentioned earlier, the narrow dimensions of the ECS make them exceptionally difficult to study, and it is reasonable that the first technique used to explore it was electron microscopy (EM). It was later recognized that chemical fixation and conventional tissue processing techniques reduce the ECS volume considerably by tissue swelling and sample dehydration, and early on an ECS preservation technique was developed by Van Harreveld and colleagues in California (Van Harreveld et al., 1965). In this pioneering work the sample was first stabilized by rapid freezing cryofixation, instead of chemical fixation by glutaraldehyde cross-linking, to prevent water loss and to immobilize structures in their hydrated state. By slowly substituting frozen water by resin, tissue blocks could be then sliced into ultrathin sections and contrasted for EM, while better preserving ECS geometry. The success of this approach relies on minimizing the time from euthanasia to cryofixation, and it works better in relatively thin tissue samples that can be rapidly frozen. An in vivo adaption has been reported, where −193 °C isopentane–propane is poured directly onto the exposed mouse brain followed by immediate slicing (Zea-Aragón et al., 2004). This allows cryofixation of superficial layers of the brain. Still, perhaps the most interesting variant of the technique is the recent use of ultrarapid high-pressure freezing (HPF) followed by freeze substitution embedding (McDonald and Auer, 2006; Sosinsky et al., 2008), a method that cryo-immobilize the parenchyma without the formation of ice crystals, therefore better preserving membranes and cellular structures. This minimizes freezing artifacts, at least in the outermost layers of tissue (Studer et al., 2008), and renders possible accurate EM snapshots of the neuropil in areas such as the mouse neocortex (Korogod et al., 2015) or the substantia nigra (Soria et al., 2020b). Beyond the outermost cortical areas, there are still no optimal approaches for fixing tissues without introducing structural artifacts. Some authors have argued, for instance, that certain cryofixation-EM estimations (e.g. astrocytic coverage of cerebral blood vessels) are in conflict with long-standing physiological data (Abbott et al., 2018). It seems plausible that the truth may therefore lie somewhere between the cryofix and chemical fixation methods.

Analysis of EM images of cryofixed tissue, or alternative ECS preservation methods that use membrane-impermeant buffers during fixation (Cragg, 1980; Kasthuri et al., 2015; Pallotto et al., 2015), revealed that the ECS represents between 15 and 20% of the parenchyma (Fig. 1A, B), and it is inhomogeneous in terms of channel widths, displaying large variations across micrometre scales. These studies found that although the average ECS width is indeed around 40–80 nm, as predicted by Thorne and Nicholson (2006), the local geometry of the ECS is highly heterogeneous, with small gaps of 10–20 nm, but also many spaces in the range of 200–500 nm (Fig. 1C). The large, several tens of nm "pools" are scattered throughout the neuropil and predictably have profound implications for diffusion (Fig. 1D). For instance, large widths were found in perisynaptic spaces, suggesting that neurotransmitter spill over can diffuse into large volumes of interstitial fluid before running into other cell membranes (Korogod et al., 2015). Similarly, an increase in the number of large pools were found after neurodegeneration (Soria et al., 2020b), suggesting that transit of small molecules is slowed down in certain areas after cell death.

EM requires tissue fixation, and despite remarkable ECS preservation by the described cryofixation techniques, EM is limited to providing single snapshots of a highly dynamic neuropil. Furthermore, since the tissue is lifeless, no experimental intervention is possible after imaging, and no physiological diffusion can be measured. Here, live imaging using fluorescence microscopy comes to the rescue. Laser-scanning microscopy modalities, such as confocal and 2-photon microscopy, provide high lateral resolution and good optical sectioning (although axial resolution is significantly worse than in the *x*-*y* plane), and have been used to visualize the live ECS. However, extracting geometrical ECS data is still difficult because of the diffraction-limited resolution of these techniques, rooted in the diffraction of light (Abbe, 1882). At around 250 nm, this limit prevents the vast majority of ECS channels from being resolved, and renders the ECS a largely homogenous blur. Still, by labelling the ISF with a membrane-impermeant fluorophore, researchers have been able to visualize in vivo the ECS with two-photon excitation (Iliff et al., 2013; Kitamura et al., 2008; Kuo et al., 2020; Xie et al., 2013), even if fine ECS details cannot be resolved. The work of Kitamura is particularly interesting, as they used the ECS labelling to visualize somata as shadows, and target these for patch-clamp in vivo. Again, dendrites, spines, or glial processes appeared too blurry to be discernible.

Super-resolution microscopy has proven critical to overcome this optical resolution limitation, and among the myriad of modalities that

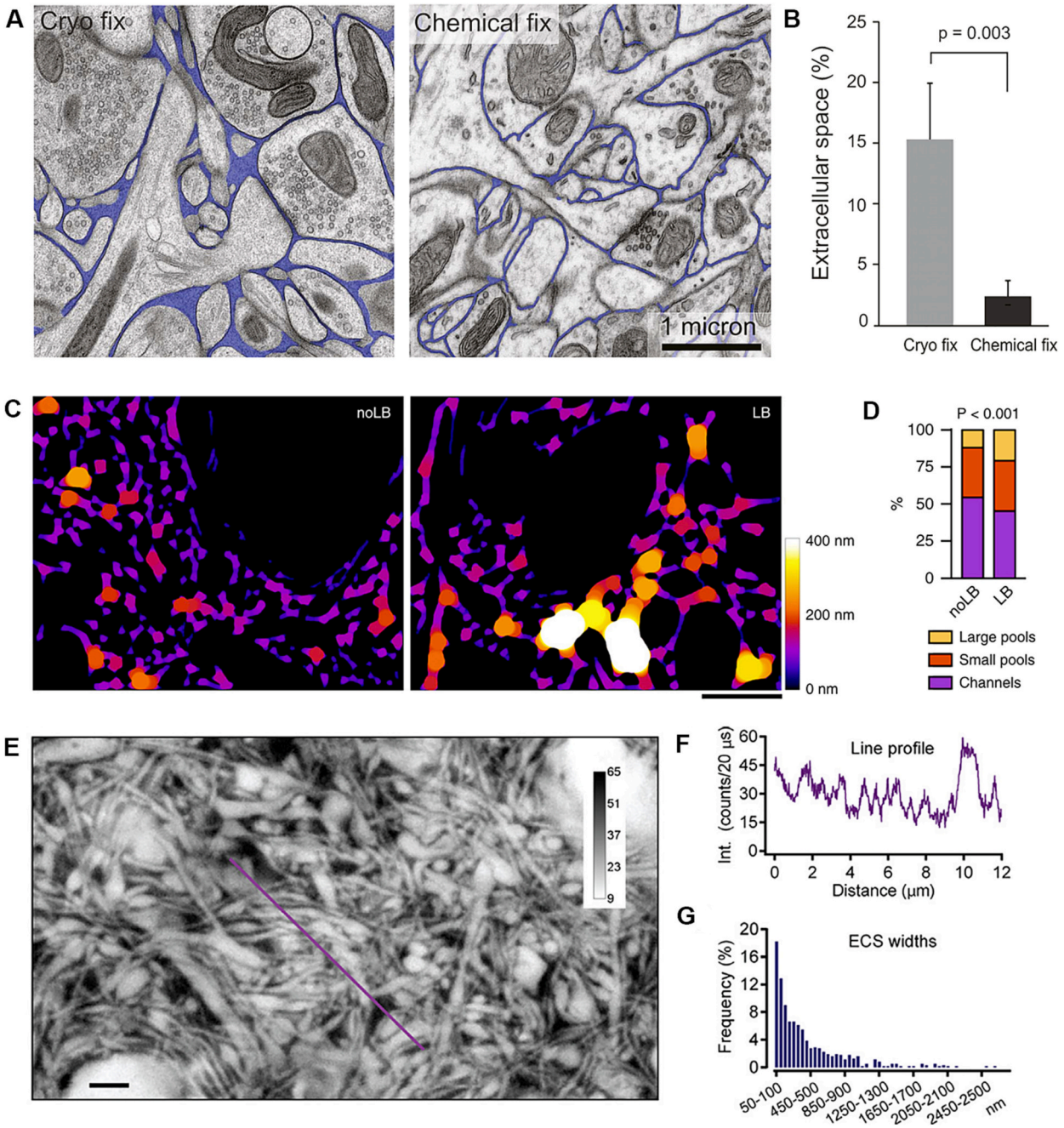

Fig. 1. Nanoscale imaging of the brain ECS. (A) Electron micrographs of high-pressure cryo-fixed vs. aldehyde-fixed mouse neocortex. Cryo-fixation allows for better preservation of ECS dimensions, since tissue structures retain their original hydrated positions. (B) The ECS volume fraction in cryo-fixed tissue is closer to physiological values (15–20%) than in chemical-fixed tissue, where the ECS shrinks. (C) Image analysis of cryofixation-EM images reveal heterogeneity of ECS dimensions in the midbrain, with a "channels" and "pools" appearance and dimensions up to 500 nm. These local ECS width maps are created from parkinsonian (*Lewy Body-injected*, or LB) and control (noLB) substantia nigra. Scale bar = 1 µm. (D) Pathology (in this case, neurodegeneration) can alter the balance of channels and pools, enlarging the ECS locally, and thereby effectively altering the ECS structure. (E) SUSHI image of the hippocampal neuropil (bright) and ECS (dark) in live tissue, revealing the complexity of the ECS compartments. Scale bar = 2 µm. (F) Intensity profile of the magenta line in (E). (G) Frequency distribution of ECS dimensions in live brain tissue, revealing a continuum of widths from 50 nm up to more than a micron. (A) and (B) are from Korogod et al., 2015, eLife. (C) and (D) are from Soria et al., 2020b, Nat Commun, both with permission (https://creativecommons.org/licenses/by/4.0/). (E) to (G) are from Tønnesen et al., 2018, Cell, with permission from Elsevier. (For interpretation of the references to colour in this figure legend, the reader is referred to the web version of this article.)

have been developed in recent years, stimulated emission depletion (STED) microscopy is particularly well-suited to image fine structures in live neural tissue (Calovi et al., 2021). Tønnesen and colleagues adopted the ISF labelling approach, though instead of pairing it with 2-photon microscopy, they used 3D-STED that has nearly a thousand-fold better volume resolution. This allowed them to visualize the ECS geometry directly, and correspondingly the cellular constituents of the neuropil as dark shadows (Tønnesen et al., 2018). An added advantage of the ISF perfusion labelling scheme is that bleached fluorophores are continuously replenished from the practically infinite reservoir of the labelled perfusion solution, thereby nearly eliminating bleaching and phototoxicity. Tønnesen and colleagues were able to observe nanoscale changes in the structure of the ECS in response to 2-photon glutamate uncaging or local tissue laser lesioning in organotypic hippocampal slices. This so

called super-resolution shadow imaging (SUSHI, Fig. 1E, F) approach offers around 50 nm lateral resolution, and has confirmed the complex organization and heterogeneous distribution of ECS geometries. Analysis of SUSHI images suggest that, rather than a classification into discrete bins of "channels" and "pools", the heterogeneity of ECS dimensions is better represented by a continuous lognormal distribution (Fig. 1G), similar to recent data from cryofixation-EM images. Whereas EM still offers higher spatial resolution, a key advantage of SUSHI is that it allows monitoring of ECS geometry in real-time and at high temporal resolution. It has been applied recently to observe nanoscale ECS changes in response to local or global stimuli, such as remodelling of astrocytic microstructure and depletion of local ECS occurring upon hypo-osmotic challenge (Arizono et al., 2021). Ongoing developments in STED microscopy to improve imaging depth and correct aberrations will facilitate similar experiments in acute slices and in vivo (Calovi et al., 2021).

3. Measuring diffusion in the brain ECS

As we mentioned earlier, the submicron dimensions of the ECS make it exceptionally difficult to study, and this hurdle has only been surpassed very recently by novel light and electron microscopy techniques (Soria et al., 2020a). Traditional methods, such as real-time iontophoresis of tetramethylammonium (RTI-TMA) and derivatives, albeit providing lower spatial resolution and limited information on ECS topology, have been the workhorse of the field since its inception, delivering a wealth of diffusional data across species, ages and experimental paradigms (Nicholson and Hrabětová, 2017; Syková and Nicholson, 2008). Diffusion measurements can be performed in a wide array of preparations, ranging from classical brain slices and newly developed brain organoids to more complex in vivo setups. While measurements in intact animals provide information closer to the ground truth, acute slices continue to be the most used preparation for their versatility and ease of use. We have summarized the strengths and limitations of the different preparations in Table 1.

It is interesting to note that some methods that measure diffusion also provide information about the ECS structure. They usually report what is known as *ECS volume fraction*, which is the ratio of ECS volume to total tissue volume within a chosen region of interest, and is often referred to as α. As we mentioned earlier, α is reportedly between 0.15 and 0.2 depending on brain region, with a tendency to decrease with age and in certain pathological conditions (Syková and Nicholson, 2008). The other parameter that is frequently used to represent the ECS structure in diffusion measurements is tortuosity (λ) (Nicholson, 2001), which is a measure of the hindrance that molecules experience while traversing the ECS. It is defined as the square root of the ratio of the free diffusion coefficient D and the effective diffusion coefficient D^*, which changes with ECS geometry and ISF constituents. Tortuosity is higher when molecules diffuse more slowly than predicted from D alone, i.e. when D^* is low:

$$\lambda = \sqrt{D/D^*} \tag{1}$$

while homogenous diffusion D remains constant for a molecule of a given radius R, at a certain temperature T and in a medium of viscosity η (k is the Boltzmann's constant):

$$D = \frac{kT}{6\pi\eta R} \tag{2}$$

Hindrance to molecular diffusion in the ECS can be also described by diffusion permeability θ (Hrabe et al., 2004), sometimes referred to as *relative diffusivity,* which is simply the ratio of D^*/D. This is a useful parameter that can be used for linear comparisons of diffusion in different media, and as shown in eq. (1), it is directly related to tortuosity when the sample is brain tissue. It should be noted, though, that in most fields the measurement of tortuosity is not derived from diffusion measurements. It just so happens that this works well for the brain ECS.

As derived from Eqs. (1) and (2), ECS tortuosity is not only determined by the size and structure of the ECS, but also by the size of the diffusing molecule and by ISF viscosity. Hence, tortuosity, and therefore diffusion permeability, is affected by obstacles that the diffusing molecule might encounter in its journey. These obstacles are the molecular constituents of the ISF, such as the dense sugars and macromolecules of the extracellular matrix. Other hurdles such as extracellular protein aggregates or plaques, especially in pathological states, might also play a role (Syková, 2004). Tortuosity is about 1.6 in isotropic brain regions such as the majority of the cerebral cortex (Lehmenkühler et al., 1993; Syková and Nicholson, 2008). However, in brain regions predominantly composed of fiber tracts, molecules diffuse more readily along the fibres than across, resulting in different values of tortuosity in these directions (Rice et al., 1993; Syková and Nicholson, 2008). Classical example is diffusion in the corpus callosum, where λ is 1.46 along the fibres and 1.72 across (Vorísek and Syková, 1997).

To measure diffusion in the ECS, RTI-TMA uses a glass micropipette to inject a precise amount of an inert molecule (in this case TMA^+) into the tissue by iontophoresis. An ion-selective microelectrode placed about 100 μm from the source micropipette measures the resulting ion concentration change as a function of time, providing a diffusion curve where the researcher can extract both α and λ by comparing the measurement to an identical measurement of free diffusion in aqueous solution (Nicholson and Phillips, 1981; Odackal et al., 2017). The ECS diffusional properties measured with the RTI method are the *average volume fraction* and the *average tortuosity* of the tissue volume that surrounds the respective source and recording electrode pair. It is, therefore, a *volume-averaging technique* that describes the ECS at the tens to hundreds of microns scale. This technique is highly versatile and has been used in brain slices and in vivo to explore the ECS properties across brain regions in neonate and adult rodents, including cortex (Mazel et al., 2002; Voříšek and Syková, 1997; Yao et al., 2008), hippocampus (Hrabětová et al., 2009; Mazel et al., 1998; McBain et al., 1990), midbrain (Cragg et al., 2001), striatum (Reum et al., 2002), and white matter (Simonová et al., 1996; Vorísek and Syková, 1997), among others.

While these studies have been conducted mostly in rodents, volume-

Table 1
Applicability, strengths and limitations of the different experimental paradigms used to measure ECS diffusivity in brain tissue, assessed at the date of manuscript preparation (December 2022). For instance, while a cultured slice allows for longer time-lapse and better optical resolution than an acute brain slice, the latter is closer to the physiological ground truth. In vivo paradigms represent the brain ECS more accurately, however electrophysiology or other concurrent techniques are more difficult to implement. Finally, while brain organoids are a highly versatile preparation, they are a relatively new model where the interstitial spaces grow without in situ patterning, and it remains unknown to what extent they recapitulate a physiological ECS as in in vivo or ex vivo brain tissue.

Experimental preparation	Physiological ground truth	Local diffusion ECS data	Achievable optical resolution	Time-lapse recordings	Ease & cost of application	Concurrent techniques
In vivo	++++	+++	+++	++++	++	++
Acute slices	+++	++++	+++	+++	+++	++++
Cultured slices	++	++++	++++	++++	++	++++
Organoids	+	++++	++++	++++	+	++++

(Best: ++++; Worst: +)

averaging methods have been used to extract ECS parameters from other species as well, first with radiotracers (1970's) and later with RTI (1980's onwards), allowing comparative studies. These other species include monkey (Blasberg et al., 1975), dog (Patlak and Fenstermacher, 1975), frog (Prokopová-Kubinová and Syková, 2000) and turtle (Rice et al., 1993), although they are often limited to one or two selected brain regions only. While measurements in turtle reported higher α (0.35) and anisotropic λ (1.44 to 1.98) in the cerebellum, all other species returned values similar to those found in rodents. Interestingly, while Cragg et al. (2001) measured an α value of 0.3 in the guinea pig midbrain using RTI-TMA, work with cryofixation-EM and carbon nanotubes in the same region, but in the mouse, found a more conventional value of 0.2 (Soria et al., 2020b).

Another point-source method, integrative optical imaging (IOI), uses a fluorophore as diffusing molecule and a widefield microscope with a fast CCD camera to visualize the diffusion gradient into the tissue from the tip of the pipette (Nicholson and Tao, 1993). This is also a volume-averaging method, and ECS geometric structure remains obscured. It enables the analysis of planar diffusion across areas defined by the effective field of view of the microscope, and it can be applied in brain slices ex vivo (Hrabetová et al., 2003) or in vivo (Thorne and Nicholson, 2006). Time-resolved IOI is a recently developed variant of the technique that improves ten-fold the measurement time resolution to around 1 Hz, allowing detection of faster fluctuations in extracellular diffusion, e.g. in the context of cortical spreading depression (Hrabe and Hrabetova, 2019). An interesting variant of the RTI method provides faster measurements, by employing an oscillating concentration of TMA^+ released at the point source in a sinusoidal time pattern. This creates diffusion waves with a particular frequency and amplitude, which are altered (delayed and attenuated) by the underlying ECS structure, providing also α and λ (Chen and Nicholson, 2002). Recent refinement in the data analysis of this technique facilitated ECS fluctuations to be resolved with high temporal resolution (Chen et al., 2019).

Microfiber imaging is a technique that resembles the RTI-TMA method, in the sense that it measures an experimental diffusion gradient between two probes. In this case, the method uses light instead of electrical current, and a membrane-impermeant fluorophore as the diffusing agent. Two micro-optical fibres measure fluorescence intensity in the overlying solution and inside the tissue, where the fluorophore distributes in the ECS. Since a proportion of the fluorophore will be displaced by cellular structures, the difference in fluorescence intensity between the tissue and the exterior will scale with the ECS volume fraction α. Despite the apparent simplicity and low cost of the method, its use has been limited, and reported by a single lab (Zhang and Verkman, 2010).

Two-photon microscopy has been used to visualize point-source diffusion of fluorescent molecules in live brain tissue. Stroh et al. (2003) calculated the diffusion parameters of a large macromolecule, nerve growth factor (NGF), by imaging rat brain slices pressure-injected with fluorophore-conjugated NGF. The researchers estimated a rather high tortuosity of 2.2 in striatum, which might be explained by the large size of NGF or by its binding to NGF receptors, which are highly expressed in the brain. The lab of Dmitri Rusakov used two-photon microscopy to measure diffusivity in acute slices in combination with electrophysiology, to address how variations in ECS diffusivity affect the activation of glutamate receptors (Savtchenko and Rusakov, 2005). In a more recent study, this team used two-photon microscopy not to investigate point-source diffusion, but instead to read out molecular rotations of a fluorophore homogenously dispersed in the ISF using polarization-sensitive optical filters. Observed variations in fluorescence polarization with respect to the polarization of the excitation laser can be attributed to differences in the ECS viscosity, and the approach can therefore be used to probe viscosity at the high spatial resolution of a 2-photon microscope. The technique, termed "time-resolved fluorescence anisotropy imaging" (TR-FAIM), is independent of fluorophore concentration and has been used to measure nanoscale diffusivity in the extracellular compartment around synapses in rat hippocampal slices (Zheng et al., 2017). Here, the authors found that molecules move, on average, 30% slower in the ECS than in free medium, and up to 46% slower inside the synaptic cleft.

Diffusion permeability inside and outside of the synaptic milieu has been a topic of great interest for years, due to its implications for synaptic transmission and neurotransmitter spillover and uptake (Barbour, 2001; Rusakov et al., 2011). More recently, nanoscopic approaches, such as single-molecule tracking, have been used to provide maps of ECS diffusivity in local environments, for example in the vicinity of the synapse (Paviolo et al., 2022). Here, researchers determined that in the immediate area around the synaptic cleft, within 500 nm of the post-synaptic density (termed "juxta-synaptic" space), molecules diffuse 10 times faster than outside this space. This study made use of carbon nanotubes as ECS fluorescent probes, tracked individually by near-infrared video microscopy, an approach pioneered by the lab of Laurent Cognet in Bordeaux that returns parallel diffusional and structural data of the ECS at super-resolution (Godin et al., 2017; Paviolo et al., 2020). Greater diffusivity measured near the synapse correlated with increased ECS dimensions, suggesting that around the cleft, the ECS is wide and diffusion is less hindered (low tortuosity). This is in agreement with cryo-fixation based EM images that show large perisynaptic spaces with narrow channels in the vicinity (Kinney et al., 2013; Korogod et al., 2015; Soria et al., 2020b). While the ECS is a perfect porous environment for nanotubes to effectively reptate (Fakhri et al., 2010), diffusivity measurements inside the cleft could be confounded by the narrow and ultra-crowded microenvironment of the synaptic cleft (Dityatev et al., 2010b), that may remain inaccessible to the nanotubes.

The size of the fluorescent molecule in single-molecule tracking approaches indeed represents a difficult conundrum for researchers. Using a smaller particle renders the fluorophore too fast and more difficult to track, whereas a more complex, larger particle, might get stuck in the narrow ECS compartments (Thorne and Nicholson, 2006). The lab of Elisabeth Nance reached a middle-ground by using 40 nm nanoparticles for multiple particle tracking in organotypic cortical slices (McKenna et al., 2021). Here, the authors examined the diffusion coefficients of nanoparticles in slices prepared from rats at different postnatal stage, and observed an inverse relationship between diffusivity and age, which the authors attributed to ECS reduction and changes in ECM composition. Although the ability to track multiple particles in a single field of view provides an advantage over other single-molecule methods, the method remains to be tested in acute slices or in vivo, where brain tissue from adult and aged animals can be used.

4. Modelling diffusion in the brain ECS

As we have just described, local diffusion in the brain ECS can be measured using various techniques, which can be spatially resolving the ECS, such as TR-FAIM or nanotube tracking, or volume-averaging, such as RTI or IOI (Soria et al., 2020a). However, TR-FAIM and nanotube tracking are not trivial techniques and can be hard to apply over larger tissue volumes. On the other hand, the volume-averaging techniques may be technically easier to apply, though their potential for revealing local diffusion is hampered by their averaging nature. To bridge the gap between these and learn about the rules that govern local ECS diffusion across various brain regions, researchers have often resorted to computational and mathematical models.

To get an intuitive understanding of extracellular diffusion and how to model it, it is helpful to consider Fick's first and second laws of diffusion. The first law states that the diffusion flux goes from higher toward lower concentrations, and that it scales with the concentration gradient. For diffusion in a single spatial dimension it can be written as

$$J = -D\frac{d\varphi}{dx} \tag{3}$$

where J is the diffusional flux, D the substance diffusion coefficient, φ the substance concentration, and x the distance along the single spatial dimension. For more spatial dimensions the general formula is written as

$$J = -D\nabla\varphi \tag{4}$$

where ∇ represents the gradient operator in multiple spatial dimensions. To further incorporate the temporal dimension we consider Fick's second law, which is written generally for diffusion in a single spatial dimension as

$$\frac{\partial C}{\partial t} = D\frac{\partial^2 C}{\partial x^2} \tag{5}$$

or for multiple spatial dimensions, as above,

$$\frac{\partial C}{\partial t} = -D\nabla^2\varphi \tag{6}$$

and where C is the concentration at time-point t, and x is the distance considered, and it assumes free diffusion in a homogenous solution.

Fick's first and second laws allow mathematical modelling of diffusion over space and time, though under the assumption that diffusion is free. However, the ECS is very complex in terms of structure and likely also viscosity, and diffusion over distances of more than a few hundreds of nanometres, at the most, cannot be considered free. On the contrary, diffusion in the brain ECS will be restricted by cellular membranes and dead spaces, by putative extracellular matrix proteins and glycans, as well as by other molecular constituents of the interstitial fluid. As molecules are released into the ECS, they begin to encounter these obstacles, resulting in a transient phase of anomalous diffusion and gradually slowing down the progress of molecules through the extracellular environment. When molecules sample a sufficient volume to encounter all types of obstacles present in a particular brain region, a normal effective diffusion coefficient is reached. This is also observed in simple geometric diffusion models, where only after a given run-time does the model λ reach a steady state (Nicholson and Kamali-Zare, 2020; Xiao et al., 2015). In the brain, anomalous diffusion was reported in rat cerebellum, where it is thought to be caused by large and geometrically complex glomeruli that act like dead spaces (Xiao et al., 2015). Determining the actual distances over which a molecular species diffuses anisotropically in other brain regions, and thereby exerts an ECS context-dependent physiological effect, will be an interesting advancement for the field.

Fick's second (and first) Law is usually modified in modelling to incorporate further spatial dimensions, geometric complexities, convective flow, cellular molecule-uptake mechanisms, space-dependency of D, and more. Experimental data on these variables is often scarce, though, and the challenge for modelers is to design the equation taking into account unknowns, while allowing a level of comparison to experimental data for model validation. Point-source diffusion in the ECS will likely always be anomalous within the first nanometres to few microns around the source point, where the heterogeneity of ECS environment is manifested. Though on larger scales, across several microns, individual sub-micron scaled effectors causing anomalous diffusion may effectively blur out, and diffusion appears normal, though obviously slower than free diffusion as determined by λ. That is, whether point-source or distributed diffusion is anisotropic or not will depend on the spatial scales that is considered.

In experimental studies that use volume-averaging RTI-TMA method, TMA diffusion curves recorded in brain are fitted with an appropriate solution of the diffusion equation to obtain effective diffusion coefficient of TMA and α (Nicholson and Phillips, 1981). Effective diffusion coefficient of TMA and free diffusion coefficient of TMA measured in a free medium are used to calculate λ (Eq. 1). Other volume averaging methods, such as IOI or TR-IOI, yield effective diffusion coefficient for the molecules studied but α is not obtained (Hrabe and Hrabetova, 2019; Nicholson and Tao, 1993). On the other hand, modelling studies commonly build an artificial ECS delimited by geometrical elements that represent cells, with their convexities and concavities, and simulate diffusion through these. Usually, the modelled indicator will be λ, as this effectively bundles geometries and viscosities, while α will be kept around 0.2 that is accepted as the overall ECS average value. From eqs. (1) and (2) we see that λ is in effect a compound term that integrates not only geometry and viscosity, but all unknown physiological factors that affect measured diffusion. Accordingly, and importantly, similar λ values can result from different combinations of ECS structure and viscosity, and therefore similar λ values do not equal similar underlying ECS properties. Similarly, identical α values may reflect very different underlying ECS structure. Another important point is that α and λ are independent parameters. Regardless of these disclaimers, it is extremely useful to know α and λ for given brain regions, to be able to compare these across experimental settings and over time. Several computational models have been put forward, trying to identify representative α and λ values for given artificial lattice structured ECS, with the aim of providing insights into the underlying ECS geometry.

One of the early attempts to model diffusion in brain tissue, by Lipinski (1990), is notable in that it is among few models based on actual microscopy images of the ECS (Lipinski, 1990). Wide-field light microscopy images of hippocampus and cortical regions from guinea pig and rat were digitized, thresholded, and binarized so that pixels represented either cellular or extracellular space, respectively. Diffusion through the resulting ECS geometry of individual particles was Monte Carlo simulated by 50 to 1000 consecutive diffusion step repetitions per particle, and the mean square displacement (MSD) was calculated and compared to Monte Carlo simulated free diffusion to obtain λ. Notably, for $\alpha = 0.2$ the model yielded on average $\lambda = 1.92$ (Lipinski, 1990). While this is on the high end compared to reported experimental values (Syková and Nicholson, 2008), it is nevertheless in the physiological range for brain tissue. The problem with this approach is that the microscope providing the images used to create this model does not offer the spatial resolution to visualize the ECS structural details, therefore the resulting cell soma-like convex geometries obtained biases the ECS structure toward larger pools, leading to higher values of λ, independently of the presence of dead-spaces.

Several models incorporate hypothetical structures representing cells arranged in lattice patterns (Fig. 2A) to explore whether ECS structural complexity is indeed sufficient to explain physiological λ values observed in brain tissue. They commonly have a high degree of structural symmetry, and therefore model a highly homogeneous tissue consisting of identical, or largely identical, cells arranged in a lattice manner. From these models it has emerged that lattices with a uniform inter-cellular distance, corresponding to a constant ECS channel width, do not readily suffice to delay diffusion to the extent observed in brain tissue (Chen and Nicholson, 2000; Hrabe et al., 2004; Tao and Nicholson, 2004). However, incorporation of diffusional dead-ends or more voluminous basins between the particles, while maintaining α around 0.2, will readily delay diffusion to the same extent as in brain tissue (Chen and Nicholson, 2000; Hrabe et al., 2004; Jin et al., 2008; Nandigam and Kroll, 2007; Tao et al., 2005). This was further explored in the context of osmotic challenge, where it was proposed that cell shrinkage leads to formation of ECS basins and a correspondingly higher α, while λ does not decrease as expected from the anti-correlation to α, due to the retention effect of basins on diffusing molecules (Chen and Nicholson, 2000).

In an oversimplified sense, the above models demonstrate that a representative tissue model with a volume fraction and geometric components reminiscent of those observed in brain parenchyma can suffice to delay diffusion to an extent observed in live brain tissue. Thus, according to these models, tortuosity can readily be dictated by ECS geometry, and therefore variations in ISF viscosity are not necessarily a determinant of λ in live tissue. The disclaimer here is that the models are not based on actual ECS geometries, and these are in reality far more complex than the model lattice or lattice-like structures, so that in reality

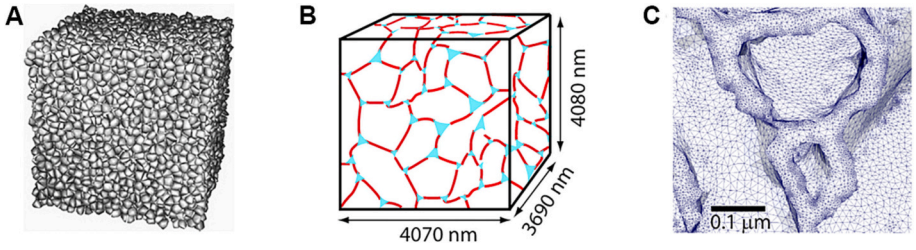

Fig. 2. Mathematical models of diffusion. (A) Random 3D ECS geometry composed of polyhedrons representing cellular elements, with diffusion allowed only between them. Monte Carlo methods are used to simulate diffusion through these lattices. Such models do not fully reflect physiological diffusion since they display a uniform ECS width, without dead-spaces. (B) A more complex ECS model, incorporating ECS width variability, can be obtained from reconstructed EM images. Pools are depicted in cyan, and channels in red. (C) Sub-micron 3D reconstruction of the ECS based on EM images. (A) is from Hrabe et al., 2004, Biophys J, with permission from Elsevier. (B) and (C) are from Holter et al., 2017, PNAS. (For interpretation of the references to colour in this figure legend, the reader is referred to the web version of this article.)

the contribution of local variations in viscosity to λ remain largely unknown. Indeed, Rusakov and Kullmann (1998) used modelling to show that viscosity will impact diffusion of small molecules through the ECS, as the presence of macromolecules in the ISF pose mechanical obstacles to diffusion analogous to obstacles in the form of cellular membranes. They proposed that λ in fact is the product of two parts, namely $\lambda_{structure}$ and $\lambda_{viscosity}$ (Rusakov and Kullmann, 1998).

The models become extremely interesting when they are used to disclose local diffusional anisotropy or complex events that cannot (yet) be revealed through wet lab experiments. Kinney et al. modelled diffusion in 180 μm^3 of hippocampal CA1 area neuropil 3D-reconstructed from electron microscopy images (Kinney et al., 2013). The measured α of the raw reconstruction was 0.08, which is lower than the predicted 0.2 value. This is likely because chemical tissue fixation is associated with swelling of cellular components and a decrease in α, which confounds ECS volume estimates in electron microscopy, as we mentioned further above (Korogod et al., 2015; Van Harreveld et al., 1965). To account for this, α was mathematically increased to produce a physiologically realistic value around 0.2. The resulting ECS structure was reported as tunnels of 40–80 nm diameter, interconnected by sheets of 10–40 nm width forming primarily between cell bodies. Monte Carlo simulations of point-source diffusion revealed that diffusion in sheets was slower than that observed in tunnels. The authors suggested, accordingly, that the specific ECS geometry in a given tissue volume may shape volume-signalling and diffusional events in general (Kinney et al., 2013).

The same 3D-reconstructed neuropil was used by others to determine tissue permeability, in order to assess whether molecular transport would occur more efficiently by diffusion or bulk flow (Holter et al., 2017) (Fig. 2B, C). Modelling suggested that transport was unlikely to occur by bulk flow under assumptions of physiological hydrostatic pressure gradients, and therefore that diffusion was the main transport mechanism, at least for this specific CA1 tissue volume. Others have disputed this observation and argued, based on modelling in a synthetic 3D ECS structure incorporating vasculature, that both diffusion and bulk flow are likely to contribute to molecular transport through the ECS (Ray et al., 2019). As these two studies apply different modelling strategies, it is difficult to accept or dismiss either of them, though we find it plausible that both bulk flow and diffusion occur, with the dominant transport mechanisms being highly dependent on the tissue volume under consideration, i.e. taking into account proximity to pulsating vessels, ECS geometry, and more. Here it is worth remembering that at least part of the brain ECS expand during sleep to facilitate metabolite clearance, which will alter tissue permeability and may transiently increase the ratio of bulk transport to diffusional transport, as shown by in vivo experiments (Xie et al., 2013).

Point-source diffusion on local scales is particularly interesting in settings of synaptic transmitter release, where usually a considerable fraction of transmitter escapes the synaptic cleft and exerts effects at neighbouring synapses or via extrasynaptic receptors. This holds true for all synaptically released transmitters, including glutamate and GABA (Kullmann, 2000). This *spillover* of transmitters occurs on sub-millisecond time-scales, and is shaped by the sub-micron spatial scales of the perisynaptic ECS geometry. Additionally it is impacted by the composition of receptor and transporter binding sites on the perisynaptic cellular structures, not least astrocytic membranes that are enriched in these (Papouin et al., 2017). As synapses are rarely symmetric or structurally isotropic, they are not well modelled by lattice structures. They are commonly so small that they are difficult to resolve by live cell compatible imaging techniques, while at the same time their structure is easily distorted by tissue fixation. Savtchenko and colleagues have modelled the impact of perisynaptic ECS geometry and astrocytic processes around glutamatergic synapses on dendritic spines (Savtchenko et al., 2021; Savtchenko and Rusakov, 2022). The model was based on spheroids randomly sized between 20 and 100 nm, which could be assigned glutamate-binding surface properties to model astrocytic glutamate transporter type 1 (GLT-1) transporters. The authors found that beyond perisynaptic ECS geometry, glutamate transporters would have a major impact on the number of glutamate molecules escaping the synapse and its immediate surroundings (Savtchenko et al., 2021; Savtchenko and Rusakov, 2022). This advanced modelling scheme contributes in understanding synapses as complex multipartite units, where signalling is moulded by a complex combination of ECS geometry, as well as local viscosities and active membrane properties. It further illustrates that modelling local diffusion in the ECS is not a straightforward task, as time scales and molecule numbers and sizes depend on the context one seeks to model, as well as the specific cell types and cellular substructures present.

Computational and mathematical modelling has highlighted concepts and plausible determinants of ECS diffusion at a broad range of scales, though the common underlying assumptions of largely homogenous and/or isotropic ECS structure and viscosity are likely an impactful confounder. We know that cells in most brain regions are arranged in recognizable patterns that likely lead to specific diffusion patterns. We also know that the constituents of the extracellular matrix are highly heterogeneously distributed and viscosity likely varies with these. In addition, point source release of transmitters and metabolites occur continuously throughout the neuropil and these will interact by enhancing or distorting local diffusion gradients. The same holds true for fluxes of water and ions across membranes that continuously alter local viscosities of the interstitial fluid. The reality is therefore a highly complex, heterogeneous, and dynamic ECS environment. As we have described further above, experimental techniques are emerging that can provide better data on local ECS geometry and viscosity in live tissue, which will facilitate development of new and more accurate diffusion models with better spatiotemporal resolution. Indeed, it appears now feasible to attempt experiments to directly compare measured and modelled point-source diffusion in the resolved ECS geometries imaged by advanced fluorescence microscopy techniques. These will boost our efforts to understand key physiological processes unfolding in the ECS, such as extracellular synaptic crosstalk, volume transmission, and metabolite clearance pathways, which we currently understand only rudimentarily.

5. What affects diffusion in the brain ECS?

Given the insights provided by both diffusion measurements and modelling described above, the current consensus is that local diffusion in the brain ECS is primarily governed by ECS geometric structure (Syková and Nicholson, 2008). Macromolecule movement is further modified by specific physicochemical characteristics, such as size or propensity for interaction with components of extracellular microenvironment. The widths of the ECS channels has been a contentious question since the 1960's when the first successful electron microscopy of the brain suggested there was exceedingly little ECS. The application of radiotracers, and today the RTI method based on volume averaging measurements have shown that the ECS occupies about 20% of brain tissue (Nicholson and Hrabětová, 2017). Estimates of ECS volume do not, however, indicate the physical dimensions and respective volume-averaging and super-resolution techniques complement each other to measure average ECS pore width in the living brain and reveal its organization at a nanoscopic level.

The complex extracellular microenvironment imposes hindrance to molecules diffusing through the ECS and therefore diffusion of substances is always slower in ECS than in free solution. Four major factors may retard local diffusion of molecules through ECS (Fig. 3): 1) geometric complexity of the ECS pathways, 2) viscosity of the interstitial fluid, including interaction with the extracellular matrix, 3) binding to membrane-bound receptors and transporters, and 4) electrochemical gradients. Resolving the effective impact on diffusion of these factors is essential to understanding the transport of molecules through the ECS, including the spread of neurotransmitters, neuromodulators and biomedically important proteins and therapeutics. We will now discuss these factors one at a time.

We will begin by asking how much the geometry of ECS hinders diffusion of molecules. When looking at an electron micrograph of brain tissue, we observe round cell bodies and ovoid cross-sections of cellular processes interspersed with elongated dendritic shafts or axons. Overall, one is left with an impression that the tissue is composed of convex elements that are separated by exceedingly narrow pores of ECS. However, recently formulated dwell-time diffusion theory (Hrabe et al., 2004; Hrabetová et al., 2003) and Monte Carlo simulations of diffusion showed that an environment filled with uniformly-spaced convex cells, ranging from a simple model composed of cubes to a more realistic one with randomly shaped convex polyhedra can explain only a portion of diffusional hindrance typically measured in brain tissue. Clearly, some other factors contribute significantly to the hindrance measured in brain ECS. One possibility is that the geometry of ECS is more complex and includes a significant amount of concavities (e.g., spaces surrounded by glial wrappings) or distended spaces (e.g., lakes). Such spaces are called dead-space microdomains and they transiently retain molecules diffusing through ECS (Hrabetová et al., 2003; Xiao et al., 2015). In fact, as commented above, when dead-space microdomains were added to the mathematical models, hindrance to diffusion increased to physiological values obtained in brain ECS. Anatomical features consistent with dead-space microdomains were found in electron micrographs of fixed brain tissue (Cragg, 1979; Grosche et al., 1999; Korogod et al., 2015; Kosaka and Hama, 1986; Spacek, 1985; Van Harreveld et al., 1965) and more recently in living brain tissue with super-resolution shadow imaging (Arizono et al., 2021). Dwell-time diffusion theory postulates that the ECS hindrance is inversely proportional to the amount of ECS contained in dead-space microdomains and it predicts that about 40% of ECS volume resides in these compartments (Hrabe et al., 2004). Because the new super-resolution imaging techniques have a capability to resolve ECS structure and function at a nanoscopic level (Godin et al., 2017; Tønnesen et al., 2018), they have the potential to not only test these quantitative predictions, but also link dead-space microdomains to putative specific cellular elements and discover the role of these in synaptic transmission and neuronal function in health and disease.

The majority of signalling molecules in the brain have their target receptors or transporters expressed on the cell surface. High-affinity binding to such targets effectively delays diffusion, and thus is a direct aspect of diffusion (Nicholson, 1995). Additionally, electrochemical gradients and local electric fields may alter nanoscale *electrodiffusion* of charged molecules in the ECS (Savtchenko et al., 2017). While these elements might influence diffusion of molecules through ECS, they are less studied, and therefore its contribution is less clear than the viscosity of the ISF, which is any hindrance to diffusion that is based on molecular ISF constituents rather than ECS geometry. Quantification of the viscosity factor is of paramount importance, since it will not only influence diffusion of molecules over a few micrometers, as geometry does, but also diffusion of neurotransmitters in narrow compartments such as the

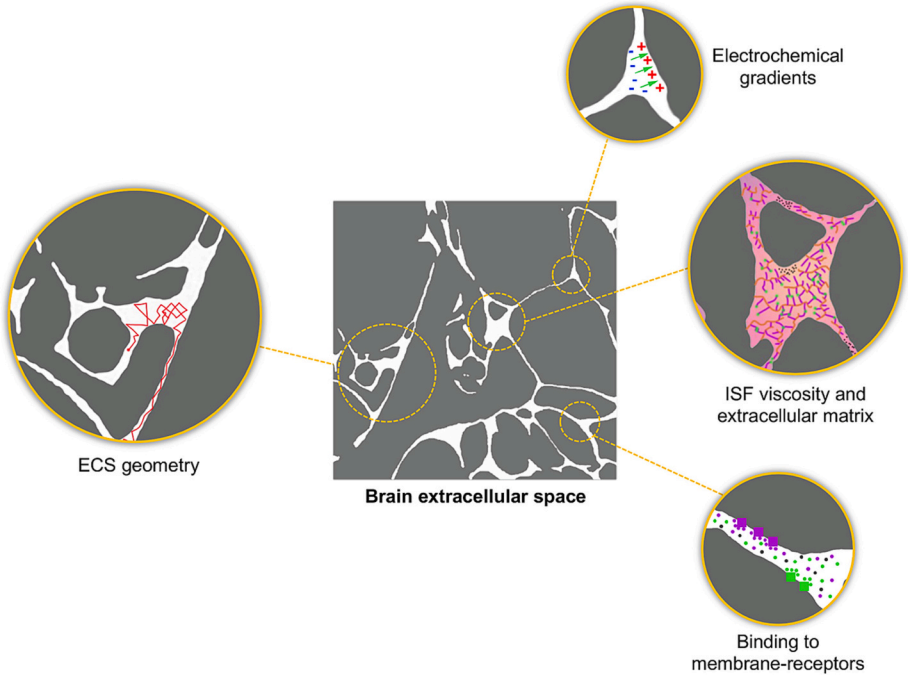

Fig. 3. Determinants of diffusion in the brain ECS. Four major factors hinder diffusion of molecules through the ECS: 1) *ECS geometry* is directly linked to volume fraction and tortuosity. A molecule diffusing through the ECS encounters a continuum of shapes and sizes, with varying degrees of geometric complexity. For instance, while channels offer a direct pathway for movement, dead-end pores or pools retain molecules transiently. 2) The *viscosity* of the interstitial fluid (ISF) is the diffusional hindrance based on molecular ISF constituents rather than geometry. The interactions with the hyaluronan and proteoglycan-rich *extracellular matrix* play a major part as a diffusion barrier, in particular to large molecules. 3) *Binding* to membrane receptors and transporters and 4) local *electrochemical gradients* also affect diffusion, of high-affinity ligands and charged molecules respectively. ECS diagram is a segmented image modified from Korogod et al., 2015, eLife (https://creativecommons.org/licenses/by/4.0/).

synaptic cleft. This will determine the timing of activation of appropriate receptors in the cleft and influence synaptic transmission. Until recently, when neuroscientists considered the diffusion of a neurotransmitter of interest, e.g. glutamate, they usually adopted one of two approaches: 1) use the *D* of glutamate (Longsworth, 1953) and lower its value by macroscopic hindrance value (Barbour, 2001), or 2) simply reduce the *D* of glutamate by about 50% (Franks et al., 2003; Nielsen et al., 2004; Rusakov, 2001; Zheng et al., 2008). However, when Rusakov's team utilized TR-FAIM to measure ISF diffusivity in living brain tissue, they found that the ISF diffusivity in hippocampal CA1 region is reduced by 30% compared to diffusivity in artificial cerebrospinal fluid, which can be ascribed to viscosity differences between the two fluids (Zheng et al., 2017). This effect was even more pronounced inside the cleft of hippocampal mossy fiber synapses where diffusivity was reduced by 46%. This study, however, did not address the origin of these differences in ISF viscosity, which is a pending question in the field.

When considering the nanoscale dimensions of the ECS, one can argue that ISF viscosity might not always be similar to the one from the cerebrospinal fluid. For instance, signalling or metabolic events such as local exocytosis of cytokines, (Stanley and Lacy, 2010) or in situ cleavage of ECM glycans (Gaudet and Popovich, 2014), may transiently and locally alter the viscosity of the ISF. Its most abundant constituent, the sugar-rich brain ECM, is a cell-membrane anchored meshwork of glycosaminoglycans, primarily hyaluronan together with negatively charged heparan sulphate and chondroitin sulphate. These components are interconnected by small link proteins to assemble a complex matrix of yet unknown density. It is involved in many biological processes including brain development, growth factor signalling, cell proliferation, migration, plasticity and homeostasis (Dityatev et al., 2010a; Lau et al., 2013; Smith et al., 2015; Yamaguchi, 2000). It is generally accepted that the interstitial matrix, which is the most abundant form of ECM in the brain, has the largest impact on ECS diffusivity (Nicholson and Hrabětová, 2017; Syková and Nicholson, 2008). On the other hand, specialized matrix structures such as the perineuronal nets (PNNs) or the perinodal ECM have been proposed to have also an impact on local diffusion of ions (Fawcett et al., 2019), since they contain an ultra-dense array of chondroitin sulphate residues. Despite much speculation about this subject, studies directly linking ECS diffusion and either PNNs (Sucha et al., 2020) or perinodal matrix (Bekku et al., 2010) are still scarce. Some studies have reported changes in ECS properties after genetic knock-out of structural components of both the interstitial and perineuronal matrix, such as link proteins Bral1 (Bekku et al., 2010) or Tenascin R (Syková et al., 2005b). However, deletion of HAS3, which synthesizes the main matrix scaffolding polymer hyaluronan, has a large impact on both interstitial matrix and ECS diffusivity, while not significantly affecting PNNs (Arranz et al., 2014).

Hyaluronan is anchored to cell membranes and forms large sugar chains that when released, increase the viscosity of the surrounding medium (Tian et al., 2013). While hyaluronan maintains the patency of the ECS thanks to its considerable hydration capacity (Arranz et al., 2014; Toole, 2004), negatively charged glycosaminoglycans may interact with positively charged substances diffusing through ECS, although this effect might be relevant in large ECS spaces, away from high-density negative charges at cell membranes. It has been shown that fast-reversible binding between the protein lactoferrin and heparan sulphate slows its extracellular transport in neocortex in vivo (Thorne et al., 2008). Hindrance for lactoferrin was significantly higher than predicted for an inert macromolecule of the same size, but this difference disappeared when co-injected glycomimetic heparin prevented an interaction between lactoferrin and heparan sulphate. By contrast, the increased hindrance was not seen with transferrin, a protein similar in structure to lactoferrin but lacking binding sites for heparan sulphate. In another example, calcium mobility was reduced by a charge-based interaction with chondroitin sulphate in acute brain slices (Hrabětová et al., 2009), since diffusion was enhanced when the tissue was treated with chondroitinase ABC. We note that the charge-based interaction was not observed for a diffusing monovalent cation TMA, suggesting that only strongly charged ions such as calcium can overcome screening of negative charges in the extracellular environment. These results suggest that chondroitin sulphate plays an important role in determining the local diffusion and concentration of calcium in brain tissue and may therefore impact synaptic transmission as well as other physiological processes. Functional coupling of calcium and chondroitin sulphate may be of significance in brain repair where both of these substances play distinct roles.

Super-resolution single-particle tracking techniques have provided new and unique information about the nanostructure of ECS and the role of hyaluronan in local diffusion. Studies in acute brain slices from young rats (Godin et al., 2017) and adult mice (Soria et al., 2020b) showed a great deal of variation in an instantaneous diffusion coefficient extracted from individual trajectories of 500 nm-long carbon nanotubes, implying heterogeneity in ECS nanostructure as well as in local viscosity. Interestingly, modification of ECS structure, both by pretreatment with hyaluronidase or inhibition of hyaluronan synthesis, did not impact heterogeneity of ECS parameters but carbon nanotubes explored larger areas of ECS with lower local viscosity and increased instantaneous diffusion coefficient. Another interesting study employed multiple particle tracking of polystyrene nanoparticles to measure their diffusion through ECS of organotypic brain slices from rats aged from 2 weeks to 2 months (McKenna et al., 2021). They reported that the effective diffusion coefficient of these 40 nm-wide particles significantly decreased as animals matured. This is likely due to a decrease of ECS volume (Lehmenkühler et al., 1993) as well as an increase in both interstitial hyaluronan (Reed et al., 2018) and the dense matrix of perineural nets (Pizzorusso et al., 2002) during maturation. Cleaving components of extracellular matrix with either chondroitinase ABC or hyaluronidase caused a significant two-fold increase of effective diffusion coefficient of nanoparticles. We cannot exclude that changes in ECS diffusivity after ECM manipulation may derive from alterations to cell-ECM attachment sites, which might alter tissue structure and therefore ECS width. Although these recent studies start to reveal the importance of the ECM on local transport through the ECS, it remains an understudied component of this brain compartment.

6. Diffusion in the brain ECS is altered in disease states

Of particular interest for pathologists is the fact that the matrix is altered in disease states in a long-lasting manner (e.g. in the form of a glial scar), thus affecting ECS parameters enduringly. Changes in ECS geometry, on the contrary, can be fast and short-lived (e.g. transient astrocyte swelling), or long-term (e.g. new dendritic spine growth). We still do not fully grasp the dynamics of the myriad of matrix components, i.e. turnover rate. Thus, we cannot compare it with the quick impact of cell movement or cell death affecting ECS geometry. However, we do know that brain tissue undergoes considerable remodelling in pathology and, especially in chronic diseases, this structural rebuilding can be persistent. We will discuss in this section how these alterations affect ECS parameters both in acute or chronic disease states.

Transient reductions in α and increases in λ have been reported, for instance, in brain ischemia/anoxia (Fig. 4A) (Hrabetová et al., 2003; Thorne and Nicholson, 2006; Vorišek and Syková, 1997), usually related to elevated extracellular K^+ and glutamate concentrations. Although both glia and neurons swell under these conditions, it has been proposed that astrocytic volume changes caused by water influx, mediated either by aquaporin-4 (Shi et al., 2017) or the Na^+/K^+ ATPase (Walch et al., 2020), are the main elements responsible for the ECS shrinkage. Furthermore, diffusion studies provide experimental evidence that dead-space microdomains, newly formed due to cell swelling, contribute to ECS hindrance in brain tissue under ischemic conditions (Hrabetová et al., 2003). Interestingly, cell death and inflammation following ischemia/reperfusion alters ECS differently, rendering a larger α,

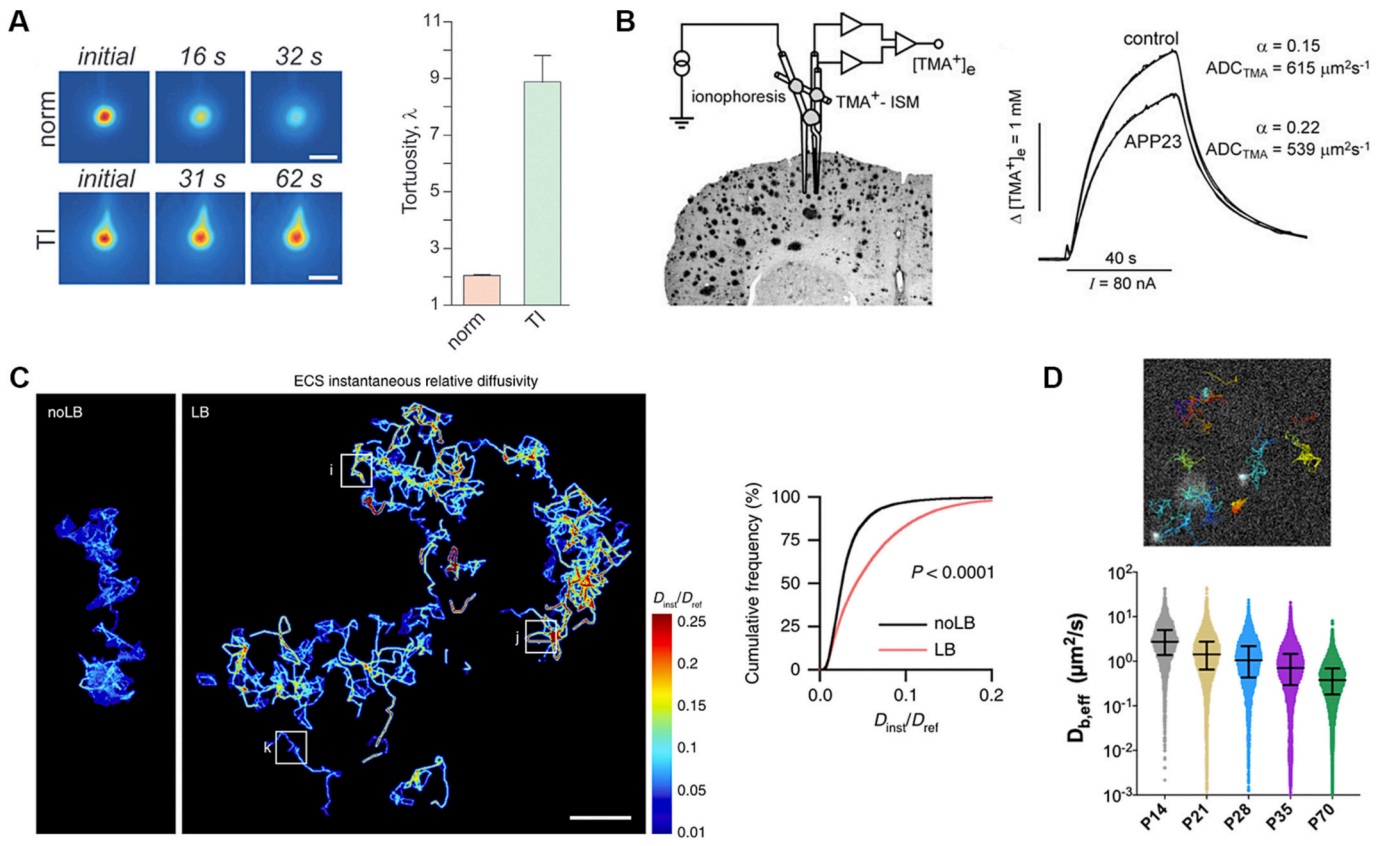

Fig. 4. Diffusion in the brain ECS is altered in pathology and aging. (A) IOI in vivo diffusion measurements revealed a several-fold increase in ECS tortuosity measure with dextran (3 kDa) in rat cortex after terminal ischemia. (B) RTI-TMA was used to measure diffusion in the cortex of aged APP23 mice, loaded with amyloid plaques. Diffusion curves showed that although ECS volume fraction was increased, diffusivity of TMA was reduced. (C) Single-nanotube tracking revealed that nanoscale diffusivity is augmented in the ECS of parkinsonian (LB) substantia nigra, compared to control (noLB) mice, where no dopaminergic neurodegeneration is present. Scale bar = 2 μm. (D) Multiple particle tracking revealed that diffusivity in the ECS decreases with developmental age, in the cortex of rats. (A) is from Thorne and Nicholson, 2006, PNAS. (B) is from Syková et al., 2005a, PNAS. (A) and (B) are Copyright (2008) National Academy of Sciences. (C) is from Soria et al., 2020b, Nat Commun, with permission (https://creativecommons.org/licenses/by/4.0/). (D) is from McKenna et al., 2021, ACS Nano, with permission.

probably caused by cell death, while counterintuitively increasing tortuosity, plausibly as a result of glial activation (Anderova et al., 2011). It should be noted that these observations were made in rats, and results may vary in other species. A fine example is the naked mole rat (*Heterocephalus glaber*), an animal that shows remarkable resilience to extreme anoxic conditions (Kim et al., 2011) and produces supercoiled hyaluronan molecules of higher molecular weight than any other animal (Kulaberoglu et al., 2019; Tian et al., 2013). A recent study employing RTI and IOI showed that the brain ECS of the naked mole rat does not shrink under ischemia, preserving diffusivity across brain tissue in conditions where in the rat brain it would normally decrease (Thevalingam et al., 2021). Since preserved diffusion permeability ensures nutrient transport even in these severe conditions, this unconventional ECS response is likely an adaptation to extreme environments.

Similar ECS changes induced by alteration of local ion concentration and astrocyte swelling occur in gliomas and epilepsy. ECS shrinkage reaches 35% during epileptiform activity (Slais et al., 2008; Tønnesen et al., 2018), and the associated increase in local glutamate concentration facilitates neuronal hyperexcitability (Murphy et al., 2017). Combining RTI-TMA and probe transients quantification (PTQ) methods showed that, in addition to the persistent reduction in α observed during epileptiform activity, the ECS volume also fluctuates rapidly, in an event termed *rapid volume pulsation* (Colbourn et al., 2021). This study also reported that both the persistent reduction of ECS and the rapid volume pulsation are eliminated by 4,4′-diisothiocyano-2,2′-stilbenedisulfonic acid (DIDS) that targets the electrogenic sodium/bicarbonate cotransporter NBCe1. Importantly, DIDS also stopped epileptiform activity. Although epileptic seizures also arise from hyperexcitability emerging from brain tumours, in human gliomas the ECS volume was reported to be increased, instead of shrunk, with a positive correlation between α and the malignancy grade (Vargová et al., 2003). This enlarged α was found mostly in the interface between astrocytomas and the surrounding tissue, and the authors explained it as the result of excitotoxic cell death, common in these tumours (Ye and Sontheimer, 1999). These larger ECS volumes, however, were not associated with a decrease in tortuosity, but a significant increase instead (Vargová et al., 2003). The overproduction of parenchymal matrix molecules by glioma cells (for a review, we refer to (Ferrer et al., 2018)), in particular hyaluronan, might create additional diffusional barriers, increasing hindrance, and therefore λ.

Another example of enlarged ECS volume fraction accompanied by increased tortuosity is found in APP23 mice (Syková et al., 2005a), which produces amyloid plaques extensively and is used to model Alzheimer's disease. Here, the authors used RTI-TMA and diffusion-weighted magnetic resonance imaging (DW-MRI) to measure and extract diffusivity from control and transgenic mice in vivo, and found that despite a larger ECS α, diffusivity was reduced (Fig. 4B). This unusual relation between α and tortuosity was also observed in another Alzheimer's disease model, the 3xTg mice (Tureckova et al., 2022). This discrepancy has been hypothesized to be the result of an enlarged ECS due to amyloid deposition, which would also create an additional diffusion barrier that increases tortuosity. Interestingly, the initial study by Syková and colleagues reported decreased ECS volume and diffusion permeability with age, more significant in females than in males (Syková et al., 2005a). The authors hypothesized that reduced ECS size in aging

might be due to reduced content of proteoglycans, which has been found in aged mice (Foscarin et al., 2017), while some authors have reported, on the contrary, hyaluronan accumulation with age in cortex and cerebellum (Reed et al., 2018). This conundrum remains, since no detailed study to date has explored the interplay between ECS and ECM in aging or Alzheimer's disease.

One study that did address this ECS-ECM interaction in pathology used single-particle tracking of carbon nanotubes together with ECS-preserving electron microscopy to study the nanoscopic structure of ECS in a mouse model of α-synuclein-induced neurodegeneration (Soria et al., 2020b). The study reported three main changes in ECS nanostructure: locally enlarged ECS volume and channel widths, increased local diffusion of carbon nanotubes (Fig. 4C), and hyaluronan deficiency in areas where microglia were activated. In a next set of experiments, it was tested whether modification of ECS structure and hyaluronan, as done previously (Godin et al., 2017), would impact the pathology. It was found that supplying small segments of hyaluronan, either by acutely cleaving hyaluronan or by direct delivery, reduced α-synuclein and dopaminergic cell loss. Taken together, this work showed that not only diffusion through the ECS, but also microglia, play a role in the clearance of toxic molecules, and suggested matrix manipulation as a target for therapy. Since ECS diffusivity decreases with age (McKenna et al., 2021, Fig. 4D), enhancing diffusion through matrix modification might also be relevant for aging studies.

Finally, we would like to address the glial scar, a physical and chemical barrier composed mostly of reactive astrocytes and a dense ECM that completely alters the local microenvironment in the border of brain injuries, ischemic cores or regions undergoing neurodegeneration (Adams and Gallo, 2018). Despite the importance of this fibrotic structure in pathology, in particular for regeneration of the damaged CNS, diffusion along the glial scar has only been sparsely studied, with most insights obtained from models of spinal cord injury [for a recent review, please refer to (Bradbury and Burnside, 2019)]. Scar-forming astrocytes occupy the injury border and, as producers on brain ECM, upregulate matrisome genes and generate a fibrous matrix around the lesioned parenchyma (Didangelos et al., 2016). A study in mice subjected to experimental stroke suggested that, while a dense glial scar is present in the penumbra of the ischemic region, it is still permeable to neurotoxic substance diffusing through the ISF (Zbesko et al., 2018). While high-molecular weight hyaluronan has been reported to accumulate on the border of demyelinating lesions (Back et al., 2005; Haindl et al., 2019), no studies have reported ECS diffusional parameters in injured white matter. Additionally, it is uncertain how the glial scar surrounding invasive experimental or therapeutic probes might hinder diffusion in the vicinity of such probes. It is plausible that astrogliosis and ECM deposition around intracerebral probes, like the ones used clinically for deep brain stimulation or experimentally for microdialysis, affect concentration measurements, especially when dealing with molecules of large size.

7. Future perspectives and pending questions

It may be argued that less is known about the extracellular space (ECS) than any other major compartment of the brain. However, the contribution of new technologies (e.g. superresolution imaging, time-resolved approaches), combined with a continuous improvement of proven paradigms (e.g. mathematical models, tissue-structure preserving fixation for EM), is constantly delivering increasingly valuable information about how molecules diffuse locally and globally in the brain ECS, along with fine details of the ECS structure and topology. These techniques will predictably get even better in the coming years, for example with improvements in temporal timescale resolution for IOI, or the combination of SUSHI and TR-FAIM to provide super-resolution maps of diffusivity along with geometrical data.

As the field continues to refine its methods and technologies, unsolved questions may become answerable. For instance, it is unknown whether highly motile microglia modulate ECS geometries locally, and what happens in pathological states where glia become reactive. We do not yet grasp the ranges of spatial and temporal scales on which ECS structural dynamics occur, or how to translate these dynamics into changes in local ECS diffusivity. Finally, the study of the dynamics of ECM composition, and how it shapes local diffusion and tortuosity in the ECS, is still in its infancy. It appears evident that the ongoing advances in live imaging techniques will help reveal these challenging enigmas, and it is already certain that ECS exploration in live tissue has entered the realm of the nanoworld. We now have, in nanoscale live imaging, an increasingly bright beacon to illuminate this *final frontier* of neuroscience.

Data availability

No data was used for the research described in the article.

Acknowledgements

The authors acknowledge funding from the Spanish Ministry of Science and Innovation (PID2020-115896RJ-I00, PID2020-113894RB-I00, PCI2022-135040-2), the Basque Government (GIC21/76, GIU21/048), CIBERNED, Human Frontier Science Program (RGP0036/2020) and Aligning Science Across Parkinson's (ASAP-020505) through the Michael J. Fox Foundation for Parkinson's Research (MJFF).

References

Abbe, H., 1882. The relation of aperture and power in the microscope*. J. R. Microsc. Soc. 2, 300–309. https://doi.org/10.1111/j.1365-2818.1882.tb00190.x.

Abbott, N.J., Pizzo, M.E., Preston, J.E., Janigro, D., Thorne, R.G., 2018. The role of brain barriers in fluid movement in the CNS: is there a "glymphatic" system? Acta Neuropathol. 135, 387–407. https://doi.org/10.1007/s00401-018-1812-4.

Adams, K.L., Gallo, V., 2018. The diversity and disparity of the glial scar. Nat. Neurosci. 21, 9–15. https://doi.org/10.1038/s41593-017-0033-9.

Anderova, M., Vorisek, I., Pivonkova, H., Benesova, J., Vargova, L., Cicanic, M., Chvatal, A., Sykova, E., 2011. Cell death/proliferation and alterations in glial morphology contribute to changes in diffusivity in the rat hippocampus after hypoxia-ischemia. J. Cereb. Blood Flow Metab. 31, 894–907. https://doi.org/10.1038/jcbfm.2010.168.

Arizono, M., Inavalli, V.V.G.K., Bancelin, S., Fernández-Monreal, M., Nägerl, U.V., 2021. Super-resolution shadow imaging reveals local remodeling of astrocytic microstructures and brain extracellular space after osmotic challenge. Glia 69, 1605–1613. https://doi.org/10.1002/glia.23995.

Arranz, A.M., Perkins, K.L., Irie, F., Lewis, D.P., Hrabe, J., Xiao, F., Itano, N., Kimata, K., Hrabetova, S., Yamaguchi, Y., 2014. Hyaluronan deficiency due to Has3 Knock-out causes altered neuronal activity and seizures via reduction in brain extracellular space. J. Neurosci. 34, 6164–6176. https://doi.org/10.1523/JNEUROSCI.3458-13.2014.

Back, S.A., Tuohy, T.M.F., Chen, H., Wallingford, N., Craig, A., Struve, J., Luo, N.L., Banine, F., Liu, Y., Chang, A., Trapp, B.D., Bebo, B.F., Rao, M.S., Sherman, L.S., 2005. Hyaluronan accumulates in demyelinated lesions and inhibits oligodendrocyte progenitor maturation. Nat. Med. 11, 966–972.

Barbour, B., 2001. An evaluation of synapse independence. J. Neurosci. 21, 7969–7984.

Bekku, Y., Vargová, L., Goto, Y., Vorísek, I., Dmytrenko, L., Narasaki, M., Ohtsuka, A., Fässler, R., Ninomiya, Y., Syková, E., Oohashi, T., 2010. Bral1: its role in diffusion barrier formation and conduction velocity in the CNS. J. Neurosci. 30, 3113–3123. https://doi.org/10.1523/JNEUROSCI.5598-09.2010.

Blasberg, R.G., Patlak, C., Fenstermacher, J.D., 1975. Intrathecal chemotherapy: brain tissue profiles after ventriculocisternal perfusion. J. Pharmacol. Exp. Ther. 195, 73–83.

Bohr, T., Hjorth, P.G., Holst, S.C., Hrabětová, S., Kiviniemi, V., Lilius, T., Lundgaard, I., Mardal, K.-A., Martens, E.A., Mori, Y., Nägerl, U.V., Nicholson, C., Tannenbaum, A., Thomas, J.H., Tithof, J., Benveniste, H., Iliff, J.J., Kelley, D.H., Nedergaard, M., 2022. The glymphatic system: current understanding and modeling. iScience 25, 104987. https://doi.org/10.1016/j.isci.2022.104987.

Bradbury, E.J., Burnside, E.R., 2019. Moving beyond the glial scar for spinal cord repair. Nat. Commun. 10, 3879. https://doi.org/10.1038/s41467-019-11707-7.

Calovi, S., Soria, F.N., Tønnesen, J., 2021. Super-resolution STED microscopy in live brain tissue. Neurobiol. Dis. 156, 105420.

Chen, K.C., Nicholson, C., 2000. Changes in brain cell shape create residual extracellular space volume and explain tortuosity behavior during osmotic challenge. Proc. Natl. Acad. Sci. U. S. A. 97, 8306–8311. https://doi.org/10.1073/pnas.150338197.

Chen, K.C., Nicholson, C., 2002. Measurement of diffusion parameters using a sinusoidal iontophoretic source in rat cortex. J. Neurosci. Methods 122, 97–108. https://doi.org/10.1016/s0165-0270(02)00299-6.

Chen, K.C., Zhou, Y., Zhao, H.-H., 2019. Time-resolved quantification of the dynamic extracellular space in the brain during short-lived event: methodology and simulations. J. Neurophysiol. 121, 1718–1734. https://doi.org/10.1152/jn.00347.2018.

Colbourn, R., Hrabe, J., Nicholson, C., Perkins, M., Goodman, J.H., Hrabetova, S., 2021. Rapid volume pulsation of the extracellular space coincides with epileptiform activity in mice and depends on the NBCe1 transporter. J. Physiol. 599, 3195–3220. https://doi.org/10.1113/JP281544.

Cragg, B., 1979. Brain extracellular space fixed for electron microscopy. Neurosci. Lett. 15, 301–306. https://doi.org/10.1016/0304-3940(79)96130-5.

Cragg, B., 1980. Preservation of extracellular space during fixation of the brain for electron microscopy. Tissue Cell 12, 63–72. https://doi.org/10.1016/0040-8166(80)90052-x.

Cragg, S.J., Nicholson, C., Kume-Kick, J., Tao, L., Rice, M.E., 2001. Dopamine-mediated volume transmission in midbrain is regulated by distinct extracellular geometry and uptake. J. Neurophysiol. 85, 1761–1771. https://doi.org/10.1152/jn.2001.85.4.1761.

Didangelos, A., Puglia, M., Iberl, M., Sanchez-Bellot, C., Roschitzki, B., Bradbury, E.J., 2016. High-throughput proteomics reveal alarmins as amplifiers of tissue pathology and inflammation after spinal cord injury. Sci. Rep. 6, 21607. https://doi.org/10.1038/srep21607.

Dityatev, A., Schachner, M., Sonderegger, P., 2010a. The dual role of the extracellular matrix in synaptic plasticity and homeostasis. Nat. Rev. Neurosci. 11, 735–746. https://doi.org/10.1038/nrn2898.

Dityatev, A., Seidenbecher, C.I., Schachner, M., 2010b. Compartmentalization from the outside: the extracellular matrix and functional microdomains in the brain. Trends Neurosci. 33, 503–512. https://doi.org/10.1016/j.tins.2010.08.003.

Fakhri, N., MacKintosh, F.C., Lounis, B., Cognet, L., Pasquali, M., 2010. Brownian motion of stiff filaments in a crowded environment. Science 330, 1804–1807. https://doi.org/10.1126/science.1197321.

Fawcett, J.W., Oohashi, T., Pizzorusso, T., 2019. The roles of perineuronal nets and the perinodal extracellular matrix in neuronal function. Nat. Rev. Neurosci. 20, 451–465.

Ferrer, V.P., Moura Neto, V., Mentlein, R., 2018. Glioma infiltration and extracellular matrix: key players and modulators. Glia 66, 1542–1565.

Foscarin, S., Raha-Chowdhury, R., Fawcett, J.W., Kwok, J.C.F., 2017. Brain ageing changes proteoglycan sulfation, rendering perineuronal nets more inhibitory. Aging (Albany NY) 9, 1607–1622. https://doi.org/10.18632/aging.101256.

Franks, K.M., Stevens, C.F., Sejnowski, T.J., 2003. Independent sources of quantal variability at single glutamatergic synapses. J. Neurosci. 23, 3186–3195.

Gaudet, A.D., Popovich, P.G., 2014. Extracellular matrix regulation of inflammation in the healthy and injured spinal cord. Exp. Neurol. 258, 24–34.

Godin, A.G., Varela, J.A., Gao, Z., Danné, N., Dupuis, J.P., Lounis, B., Groc, L., Cognet, L., 2017. Single-nanotube tracking reveals the nanoscale organization of the extracellular space in the live brain. Nat. Nanotechnol. 12, 238–243.

Grosche, J., Matyash, V., Möller, T., Verkhratsky, A., Reichenbach, A., Kettenmann, H., 1999. Microdomains for neuron-glia interaction: parallel fiber signaling to Bergmann glial cells. Nat. Neurosci. 2, 139–143. https://doi.org/10.1038/5692.

Haindl, M.T., Köck, U., Zeitelhofer-Adzemovic, M., Fazekas, F., Hochmeister, S., 2019. The formation of a glial scar does not prohibit remyelination in an animal model of multiple sclerosis. Glia 67, 467–481.

Hladky, S.B., Barrand, M.A., 2022. The glymphatic hypothesis: the theory and the evidence. Fluids Barriers CNS 19, 9. https://doi.org/10.1186/s12987-021-00282-z.

Holter, K.E., Kehlet, B., Devor, A., Sejnowski, T.J., Dale, A.M., Omholt, S.W., Ottersen, O. P., Nagelhus, E.A., Mardal, K.-A., Pettersen, K.H., 2017. Interstitial solute transport in 3D reconstructed neuropil occurs by diffusion rather than bulk flow. Proc. Natl. Acad. Sci. U. S. A. 114, 9894–9899. https://doi.org/10.1073/pnas.1706942114.

Hrabe, J., Hrabetova, S., 2019. Time-resolved integrative optical imaging of diffusion during spreading depression. Biophys. J. 117, 1783–1794.

Hrabe, J., Hrabetová, S., Segeth, K., 2004. A model of effective diffusion and tortuosity in the extracellular space of the brain. Biophys. J. 87, 1606–1617. https://doi.org/10.1529/biophysj.103.039495.

Hrabetová, S., Hrabe, J., Nicholson, C., 2003. Dead-space microdomains hinder extracellular diffusion in rat neocortex during ischemia. J. Neurosci. 23, 8351–8359.

Hrabětová, S., Masri, D., Tao, L., Xiao, F., Nicholson, C., 2009. Calcium diffusion enhanced after cleavage of negatively charged components of brain extracellular matrix by chondroitinase ABC. J. Physiol. 587, 4029–4049. https://doi.org/10.1113/jphysiol.2009.170092.

Iliff, J.J., Wang, M., Zeppenfeld, D.M., Venkataraman, A., Plog, B.A., Liao, Y., Deane, R., Nedergaard, M., 2013. Cerebral arterial pulsation drives paravascular CSF-interstitial fluid exchange in the murine brain. J. Neurosci. 33, 18190–18199.

Jin, S., Zador, Z., Verkman, A.S., 2008. Random-walk model of diffusion in three dimensions in brain extracellular space: comparison with microfiberoptic photobleaching measurements. Biophys. J. 95, 1785–1794. https://doi.org/10.1529/biophysj.108.131466.

Kasthuri, N., Hayworth, K.J., Berger, D.R., Schalek, R.L., Conchello, J.A., Knowles-Barley, S., Lee, D., Vázquez-Reina, A., Kaynig, V., Jones, T.R., Roberts, M., Morgan, J.L., Tapia, J.C., Seung, H.S., Roncal, W.G., Vogelstein, J.T., Burns, R., Sussman, D.L., Priebe, C.E., Pfister, H., Lichtman, J.W., 2015. Saturated reconstruction of a volume of neocortex. Cell 162, 648–661. https://doi.org/10.1016/j.cell.2015.06.054.

Kim, E.B., Fang, X., Fushan, A.A., Huang, Z., Lobanov, A.V., Han, L., Marino, S.M., Sun, X., Turanov, A.A., Yang, P., Yim, S.H., Zhao, X., Kasaikina, M.V., Stoletzki, N., Peng, C., Polak, P., Xiong, Z., Kiezun, A., Zhu, Y., Chen, Y., Kryukov, G.V., Zhang, Q., Peshkin, L., Yang, L., Bronson, R.T., Buffenstein, R., Wang, B., Han, C., Li, Q., Chen, L., Zhao, W., Sunyaev, S.R., Park, T.J., Zhang, G., Wang, J., Gladyshev, V.N., 2011. Genome sequencing reveals insights into physiology and longevity of the naked mole rat. Nature 479, 223–227. https://doi.org/10.1038/nature10533.

Kinney, J.P., Spacek, J., Bartol, T.M., Bajaj, C.L., Harris, K.M., Sejnowski, T.J., 2013. Extracellular sheets and tunnels modulate glutamate diffusion in hippocampal neuropil. J. Comp. Neurol. 521, 448–464. https://doi.org/10.1002/cne.23181.

Kitamura, K., Judkewitz, B., Kano, M., Denk, W., Häusser, M., 2008. Targeted patch-clamp recordings and single-cell electroporation of unlabeled neurons in vivo. Nat. Methods 5, 61–67. https://doi.org/10.1038/nmeth1150.

Korogod, N., Petersen, C.C., Knott, G.W., 2015. Ultrastructural analysis of adult mouse neocortex comparing aldehyde perfusion with cryo fixation. eLife 4, e05793. https://doi.org/10.7554/eLife.05793.

Kosaka, T., Hama, K., 1986. Three-dimensional structure of astrocytes in the rat dentate gyrus. J. Comp. Neurol. 249, 242–260. https://doi.org/10.1002/cne.902490209.

Krishnaswamy, V.R., Benbenishty, A., Blinder, P., Sagi, I., 2019. Demystifying the extracellular matrix and its proteolytic remodeling in the brain: structural and functional insights. Cell. Mol. Life Sci. 76, 3229–3248. https://doi.org/10.1007/s00018-019-03182-6.

Kulaberoglu, Y., Bhushan, B., Hadi, F., Chakrabarti, S., Khaled, W.T., Rankin, K.S., Smith, E.S.J., Frankel, D., 2019. The material properties of naked mole-rat hyaluronan. Sci. Rep. 9, 6632. https://doi.org/10.1038/s41598-019-43194-7.

Kullmann, D.M., 2000. Spillover and synaptic cross talk mediated by glutamate and GABA in the mammalian brain. Prog. Brain Res. 125, 339–351. https://doi.org/10.1016/S0079-6123(00)25023-1.

Kuo, S.P., Chiang, P.-P., Nippert, A.R., Newman, E.A., 2020. Spatial organization and dynamics of the extracellular space in the mouse retina. J. Neurosci. 40, 7785–7794. https://doi.org/10.1523/JNEUROSCI.1717-20.2020.

Lau, L.W., Cua, R., Keough, M.B., Haylock-Jacobs, S., Yong, V.W., 2013. Pathophysiology of the brain extracellular matrix: a new target for remyelination. Nat. Rev. Neurosci. 14, 722–729.

Lehmenkühler, A., Syková, E., Svoboda, J., Zilles, K., Nicholson, C., 1993. Extracellular space parameters in the rat neocortex and subcortical white matter during postnatal development determined by diffusion analysis. Neuroscience 55, 339–351. https://doi.org/10.1016/0306-4522(93)90503-8.

Lipinski, H.G., 1990. Monte Carlo simulation of extracellular diffusion in brain tissues. Phys. Med. Biol. 35, 441–447. https://doi.org/10.1088/0031-9155/35/3/012.

Longsworth, L.G., 1953. Diffusion measurements, at 25°, of aqueous solutions of amino acids, peptides and sugars. J. Am. Chem. Soc. 75, 5705–5709. https://doi.org/10.1021/ja01118a065.

Mazel, T., Simonová, Z., Syková, E., 1998. Diffusion heterogeneity and anisotropy in rat hippocampus. Neuroreport 9, 1299–1304. https://doi.org/10.1097/00001756-199805110-00008.

Mazel, T., Richter, F., Vargová, L., Syková, E., 2002. Changes in extracellular space volume and geometry induced by cortical spreading depression in immature and adult rats. Physiol. Res. 51 (Suppl. 1), S85–S93.

McBain, C.J., Traynelis, S.F., Dingledine, R., 1990. Regional variation of extracellular space in the hippocampus. Science 249, 674–677. https://doi.org/10.1126/science.2382142.

McDonald, K.L., Auer, M., 2006. High-pressure freezing, cellular tomography, and structural cell biology. BioTechniques 41, 137–143. https://doi.org/10.2144/000112226.

McKenna, M., Shackelford, D., Ferreira Pontes, H., Ball, B., Nance, E., 2021. Multiple particle tracking detects changes in brain extracellular matrix and predicts neurodevelopmental age. ACS Nano 15, 8559–8573. https://doi.org/10.1021/acsnano.1c00394.

Murphy, T.R., Binder, D.K., Fiacco, T.A., 2017. Turning down the volume: astrocyte volume change in the generation and termination of epileptic seizures. Neurobiol. Dis. 104, 24–32.

Nandigam, R.K., Kroll, D.M., 2007. Three-dimensional modeling of the brain's ECS by minimum configurational energy packing of fluid vesicles. Biophys. J. 92, 3368–3378. https://doi.org/10.1529/biophysj.106.095547.

Nicholson, C., 1995. Interaction between diffusion and Michaelis-Menten uptake of dopamine after iontophoresis in striatum. Biophys. J. 68, 1699–1715. https://doi.org/10.1016/S0006-3495(95)80348-6.

Nicholson, C., 2001. Diffusion and related transport mechanisms in brain tissue. Rep. Prog. Phys. 64, 815–884. https://doi.org/10.1088/0034-4885/64/7/202.

Nicholson, C., Hrabětová, S., 2017. Brain extracellular space: the final frontier of neuroscience. Biophys. J. 113, 2133–2142.

Nicholson, C., Kamali-Zare, P., 2020. Reduction of dimensionality in Monte Carlo simulation of diffusion in extracellular space surrounding cubic cells. Neurochem. Res. 45, 42–52. https://doi.org/10.1007/s11064-019-02793-6.

Nicholson, C., Phillips, J.M., 1981. Ion diffusion modified by tortuosity and volume fraction in the extracellular microenvironment of the rat cerebellum. J. Physiol. 321, 225–257.

Nicholson, C., Tao, L., 1993. Hindered diffusion of high molecular weight compounds in brain extracellular microenvironment measured with integrative optical imaging. Biophys. J. 65, 2277–2290. https://doi.org/10.1016/S0006-3495(93)81324-9.

Nielsen, T.A., DiGregorio, D.A., Silver, R.A., 2004. Modulation of glutamate mobility reveals the mechanism underlying slow-rising AMPAR EPSCs and the diffusion coefficient in the synaptic cleft. Neuron 42, 757–771. https://doi.org/10.1016/j.neuron.2004.04.003.

Odackal, J., Colbourn, R., Odackal, N.J., Tao, L., Nicholson, C., Hrabetova, S., 2017. Real-time iontophoresis with tetramethylammonium to quantify volume fraction and tortuosity of brain extracellular space. J. Vis. Exp. https://doi.org/10.3791/55755.

Pallotto, M., Watkins, P.V., Fubara, B., Singer, J.H., Briggman, K.L., 2015. Extracellular space preservation aids the connectomic analysis of neural circuits. Elife 4, e08206. https://doi.org/10.7554/eLife.08206.

Papouin, T., Dunphy, J., Tolman, M., Foley, J.C., Haydon, P.G., 2017. Astrocytic control of synaptic function. Philos. Trans. R. Soc. Lond. Ser. B Biol. Sci. 372, 20160154. https://doi.org/10.1098/rstb.2016.0154.

Patlak, C.S., Fenstermacher, J.D., 1975. Measurements of dog blood-brain transfer constants by ventriculocisternal perfusion. Am. J. Phys. 229, 877–884. https://doi.org/10.1152/ajplegacy.1975.229.4.877.

Paviolo, C., Soria, F.N., Ferreira, J.S., Lee, A., Groc, L., Bezard, E., Cognet, L., 2020. Nanoscale exploration of the extracellular space in the live brain by combining single carbon nanotube tracking and super-resolution imaging analysis. Methods 174, 91–99.

Paviolo, C., Ferreira, J.S., Lee, A., Hunter, D., Calaresu, I., Nandi, S., Groc, L., Cognet, L., 2022. Near-infrared carbon nanotube tracking reveals the nanoscale extracellular space around synapses. Nano Lett. 22, 6849–6856. https://doi.org/10.1021/acs.nanolett.1c04259.

Pizzo, M.E., Thorne, R.G., 2017. Chapter 6 - the extracellular and perivascular spaces of the brain. In: Badaut, J., Plesnila, N. (Eds.), Brain Edema. Academic Press, San Diego, pp. 105–127. https://doi.org/10.1016/B978-0-12-803196-4.00006-0.

Pizzorusso, T., Medini, P., Berardi, N., Chierzi, S., Fawcett, J.W., Maffei, L., 2002. Reactivation of ocular dominance plasticity in the adult visual cortex. Science 298, 1248–1251. https://doi.org/10.1126/science.1072699.

Prokopová-Kubinová, S., Syková, E., 2000. Extracellular diffusion parameters in spinal cord and filum terminale of the frog. J. Neurosci. Res. 62, 530–538. https://doi.org/10.1002/1097-4547(20001115)62:4<530::AID-JNR7>3.0.CO;2-7.

Rasmussen, M.K., Mestre, H., Nedergaard, M., 2018. The glymphatic pathway in neurological disorders. Lancet Neurol. 17, 1016–1024.

Ray, L., Iliff, J.J., Heys, J.J., 2019. Analysis of convective and diffusive transport in the brain interstitium. Fluids Barriers CNS 16, 6. https://doi.org/10.1186/s12987-019-0126-9.

Reed, M.J., Damodarasamy, M., Pathan, J.L., Erickson, M.A., Banks, W.A., Vernon, R.B., 2018. The effects of normal aging on regional accumulation of hyaluronan and chondroitin sulfate proteoglycans in the mouse brain. J. Histochem. Cytochem. 66, 697–707.

Reum, T., Olshausen, F., Mazel, T., Vorísek, I., Morgenstern, R., Syková, E., 2002. Diffusion parameters in the striatum of rats with 6-hydroxydopamine-induced lesions and with fetal mesencephalic grafts. J. Neurosci. Res. 70, 680–693. https://doi.org/10.1002/jnr.10332.

Rice, M.E., Okada, Y.C., Nicholson, C., 1993. Anisotropic and heterogeneous diffusion in the turtle cerebellum: implications for volume transmission. J. Neurophysiol. 70, 2035–2044. https://doi.org/10.1152/jn.1993.70.5.2035.

Rusakov, D.A., 2001. The role of perisynaptic glial sheaths in glutamate spillover and extracellular Ca(2+) depletion. Biophys. J. 81, 1947–1959. https://doi.org/10.1016/S0006-3495(01)75846-8.

Rusakov, D.A., Kullmann, D.M., 1998. Geometric and viscous components of the tortuosity of the extracellular space in the brain. Proc. Natl. Acad. Sci. 95, 8975–8980. https://doi.org/10.1073/pnas.95.15.8975.

Rusakov, D.A., Savtchenko, L.P., Zheng, K., Henley, J.M., 2011. Shaping the synaptic signal: molecular mobility inside and outside the cleft. Trends Neurosci. 34, 359–369. https://doi.org/10.1016/j.tins.2011.03.002.

Savtchenko, L.P., Rusakov, D.A., 2005. Extracellular diffusivity determines contribution of high-versus low-affinity receptors to neural signaling. Neuroimage 25, 101–111. https://doi.org/10.1016/j.neuroimage.2004.11.020.

Savtchenko, L.P., Rusakov, D.A., 2022. Increased extrasynaptic glutamate escape in stochastically shaped probabilistic synaptic environment. Biomedicines 10, 2406. https://doi.org/10.3390/biomedicines10102406.

Savtchenko, L.P., Poo, M.M., Rusakov, D.A., 2017. Electrodiffusion phenomena in neuroscience: a neglected companion. Nat. Rev. Neurosci. 18, 598–612. https://doi.org/10.1038/nrn.2017.101.

Savtchenko, L.P., Zheng, K., Rusakov, D.A., 2021. Buffering by transporters can spare geometric hindrance in controlling glutamate escape. Front. Cell. Neurosci. 15, 707813 https://doi.org/10.3389/fncel.2021.707813.

Shi, Z., Zhang, W., Lu, Yang, Lu, Yi, Xu, L., Fang, Q., Wu, M., Jia, M., Wang, Y., Dong, L., Yan, X., Yang, S., Yuan, F., 2017. Aquaporin 4-mediated glutamate-induced astrocyte swelling is partially mediated through metabotropic glutamate receptor 5 activation. Front. Cell. Neurosci. 11, 116. https://doi.org/10.3389/fncel.2017.00116.

Simonová, Z., Svoboda, J., Orkand, P., Bernard, C.C., Lassmann, H., Syková, E., 1996. Changes of extracellular space volume and tortuosity in the spinal cord of Lewis rats with experimental autoimmune encephalomyelitis. Physiol. Res. 45, 11–22.

Slais, K., Vorisek, I., Zoremba, N., Homola, A., Dmytrenko, L., Sykova, E., 2008. Brain metabolism and diffusion in the rat cerebral cortex during pilocarpine-induced status epilepticus. Exp. Neurol. 209, 145–154. https://doi.org/10.1016/j.expneurol.2007.09.008.

Smith, P.D., Coulson-Thomas, V.J., Foscarin, S., Kwok, J.C.F., Fawcett, J.W., 2015. "GAG-ing with the neuron": the role of glycosaminoglycan patterning in the central nervous system. Exp. Neurol. 274, 100–114. https://doi.org/10.1016/j.expneurol.2015.08.004.

Soria, F.N., Miguelez, C., Peñagarikano, O., Tønnesen, J., 2020a. Current techniques for investigating the brain extracellular space. Front. Neurosci. 14.

Soria, F.N., Paviolo, C., Doudnikoff, E., Arotcarena, M.-L., Lee, A., Danné, N., Mandal, A. K., Gosset, P., Dehay, B., Groc, L., Cognet, L., Bezard, E., 2020b. Synucleinopathy alters nanoscale organization and diffusion in the brain extracellular space through hyaluronan remodeling. Nat. Commun. 11, 3440. https://doi.org/10.1038/s41467-020-17328-9.

Sosinsky, G.E., Crum, J., Jones, Y.Z., Lanman, J., Smarr, B., Terada, M., Martone, M.E., Deerinck, T.J., Johnson, J.E., Ellisman, M.H., 2008. The combination of chemical fixation procedures with high pressure freezing and freeze substitution preserves highly labile tissue ultrastructure for electron tomography applications. J. Struct. Biol. 161, 359–371. https://doi.org/10.1016/j.jsb.2007.09.002. The 4th International Conference on Electron Tomography.

Spacek, J., 1985. Three-dimensional analysis of dendritic spines. III. Glial sheath. Anat. Embryol. (Berl.) 171, 245–252. https://doi.org/10.1007/BF00341419.

Stanley, A.C., Lacy, P., 2010. Pathways for cytokine secretion. Physiology 25, 218–229. https://doi.org/10.1152/physiol.00017.2010.

Stroh, M., Zipfel, W.R., Williams, R.M., Webb, W.W., Saltzman, W.M., 2003. Diffusion of nerve growth factor in rat striatum as determined by multiphoton microscopy. Biophys. J. 85, 581–588. https://doi.org/10.1016/S0006-3495(03)74502-0.

Studer, D., Humbel, B.M., Chiquet, M., 2008. Electron microscopy of high pressure frozen samples: bridging the gap between cellular ultrastructure and atomic resolution. Histochem. Cell Biol. 130, 877–889. https://doi.org/10.1007/s00418-008-0500-1.

Sucha, P., Chmelova, M., Kamenicka, M., Bochin, M., Oohashi, T., Vargova, L., 2020. The effect of Hapln4 link protein deficiency on extracellular space diffusion parameters and perineuronal nets in the auditory system during aging. Neurochem. Res. 45, 68–82. https://doi.org/10.1007/s11064-019-02894-2.

Syková, E., 2004. Extrasynaptic volume transmission and diffusion parameters of the extracellular space. Neurosci. Brain Water Homeost. 129, 861–876. https://doi.org/10.1016/j.neuroscience.2004.06.077.

Syková, E., Nicholson, C., 2008. Diffusion in brain extracellular space. Physiol. Rev. 88, 1277–1340.

Syková, E., Vořísek, I., Antonova, T., Mazel, T., Meyer-Luehmann, M., Jucker, M., Hájek, M., Or, M., Bureš, J., 2005a. Changes in extracellular space size and geometry in APP23 transgenic mice: a model of Alzheimer's disease. Proc. Natl. Acad. Sci. 102, 479–484. https://doi.org/10.1073/pnas.0408235102.

Syková, E., Vořísek, I., Mazel, T., Antonova, T., Schachner, M., 2005b. Reduced extracellular space in the brain of tenascin-R- and HNK-1-sulphotransferase deficient mice. Eur. J. Neurosci. 22, 1873–1880. https://doi.org/10.1111/j.1460-9568.2005.04375.x.

Tao, L., Nicholson, C., 2004. Maximum geometrical hindrance to diffusion in brain extracellular space surrounding uniformly spaced convex cells. J. Theor. Biol. 229, 59–68. https://doi.org/10.1016/j.jtbi.2004.03.003.

Tao, A., Tao, L., Nicholson, C., 2005. Cell cavities increase tortuosity in brain extracellular space. J. Theor. Biol. 234, 525–536. https://doi.org/10.1016/j.jtbi.2004.12.009.

Thevalingam, D., Naik, A.A., Hrabe, J., McCloskey, D.P., Hrabětová, S., 2021. Brain extracellular space of the naked mole-rat expands and maintains normal diffusion under ischemic conditions. Brain Res. 1771, 147646 https://doi.org/10.1016/j.brainres.2021.147646.

Thorne, R.G., Nicholson, C., 2006. *In vivo* diffusion analysis with quantum dots and dextrans predicts the width of brain extracellular space. Proc. Natl. Acad. Sci. U. S. A. 103, 5567–5572. https://doi.org/10.1073/pnas.0509425103.

Thorne, R.G., Lakkaraju, A., Rodriguez-Boulan, E., Nicholson, C., 2008. In vivo diffusion of lactoferrin in brain extracellular space is regulated by interactions with heparan sulfate. Proc. Natl. Acad. Sci. 105, 8416–8421. https://doi.org/10.1073/pnas.0711345105.

Tian, X., Azpurua, J., Hine, C., Vaidya, A., Myakishev-Rempel, M., Ablaeva, J., Mao, Z., Nevo, E., Gorbunova, V., Seluanov, A., 2013. High-molecular-mass hyaluronan mediates the cancer resistance of the naked mole rat. Nature 499, 346–349.

Tønnesen, J., Inavalli, V.V.G.K., Nägerl, U.V., 2018. Super-resolution imaging of the extracellular space in living brain tissue. Cell 172, 1108–1121.e15.

Toole, B.P., 2004. Hyaluronan: from extracellular glue to pericellular cue. Nat. Rev. Cancer 4, 528–539.

Tureckova, J., Kamenicka, M., Kolenicova, D., Filipi, T., Hermanova, Z., Kriska, J., Meszarosova, L., Pukajova, B., Valihrach, L., Androvic, P., Zucha, D., Chmelova, M., Vargova, L., Anderova, M., 2022. Compromised astrocyte swelling/volume regulation in the Hippocampus of the triple transgenic mouse model of Alzheimer's disease. Front. Aging Neurosci. 13, 783120 https://doi.org/10.3389/fnagi.2021.783120.

Van Harreveld, A., Crowell, J., Malhotra, S.K., 1965. A study of extracellular space in central nervous tissue by freeze-substitution. J. Cell Biol. 25, 117–137.

Vargová, L., Syková, E., 2014. Astrocytes and extracellular matrix in extrasynaptic volume transmission. Philos. Trans. R. Soc. B 369, 20130608. https://doi.org/10.1098/rstb.2013.0608.

Vargová, L., Homola, A., Zámečník, J., Tichý, M., Beneš, V., Syková, E., 2003. Diffusion parameters of the extracellular space in human gliomas. Glia 42, 77–88. https://doi.org/10.1002/glia.10204.

Vorísek, I., Syková, E., 1997. Evolution of anisotropic diffusion in the developing rat corpus callosum. J. Neurophysiol. 78, 912–919. https://doi.org/10.1152/jn.1997.78.2.912.

Vořísek, I., Syková, E., 1997. Ischemia-induced changes in the extracellular space diffusion parameters, K+, and pH in the developing rat cortex and corpus callosum. J. Cereb. Blood Flow Metab. 17, 191–203. https://doi.org/10.1097/00004647-199702000-00009.

Walch, E., Murphy, T.R., Cuvelier, N., Aldoghmi, M., Morozova, C., Donohue, J., Young, G., Samant, A., Garcia, S., Alvarez, C., Bilas, A., Davila, D., Binder, D.K., Fiacco, T.A., 2020. Astrocyte-selective volume increase in elevated extracellular potassium conditions is mediated by the Na+/K+ ATPase and occurs independently of aquaporin 4. ASN Neuro 12. https://doi.org/10.1177/1759091420967152, 1759091420967152.

Xiao, F., Hrabe, J., Hrabetova, S., 2015. Anomalous extracellular diffusion in rat cerebellum. Biophys. J. 108, 2384–2395. https://doi.org/10.1016/j.bpj.2015.02.034.

Xie, L., Kang, H., Xu, Q., Chen, M.J., Liao, Y., Thiyagarajan, M., O'Donnell, J., Christensen, D.J., Nicholson, C., Iliff, J.J., Takano, T., Deane, R., Nedergaard, M., 2013. Sleep drives metabolite clearance from the adult brain. Science 342, 373–377.

Yamaguchi, Y., 2000. Lecticans: organizers of the brain extracellular matrix. Cell. Mol. Life Sci. 57, 276–289. https://doi.org/10.1007/PL00000690.

Yao, X., Hrabětová, S., Nicholson, C., Manley, G.T., 2008. Aquaporin-4-deficient mice have increased extracellular space without tortuosity change. J. Neurosci. 28, 5460–5464. https://doi.org/10.1523/JNEUROSCI.0257-08.2008.

Ye, Z.C., Sontheimer, H., 1999. Glioma cells release excitotoxic concentrations of glutamate. Cancer Res. 59, 4383–4391.

Zbesko, J.C., Nguyen, T.-V.V., Yang, T., Frye, J.B., Hussain, O., Hayes, M., Chung, A., Day, W.A., Stepanovic, K., Krumberger, M., Mona, J., Longo, F.M., Doyle, K.P., 2018. Glial scars are permeable to the neurotoxic environment of chronic stroke infarcts. Neurobiol. Dis. 112, 63–78. https://doi.org/10.1016/j.nbd.2018.01.007.

Zea-Aragón, Z., Terada, N., Ohno, N., Fujii, Y., Baba, T., Ohno, S., 2004. Effects of anoxia on serum immunoglobulin and albumin leakage through blood–brain barrier in mouse cerebellum as revealed by cryotechniques. J. Neurosci. Methods 138, 89–95. https://doi.org/10.1016/j.jneumeth.2004.03.018.

Zhang, H., Verkman, A.S., 2010. Microfiberoptic measurement of extracellular space volume in brain and tumor slices based on fluorescent dye partitioning. Biophys. J. 99, 1284–1291.

Zheng, K., Scimemi, A., Rusakov, D.A., 2008. Receptor actions of synaptically released glutamate: the role of transporters on the scale from nanometers to microns. Biophys. J. 95, 4584–4596. https://doi.org/10.1529/biophysj.108.129874.

Zheng, K., Jensen, T.P., Savtchenko, L.P., Levitt, J.A., Suhling, K., Rusakov, D.A., 2017. Nanoscale diffusion in the synaptic cleft and beyond measured with time-resolved fluorescence anisotropy imaging. Sci. Rep. 7, 42022. https://doi.org/10.1038/srep42022.